PULSE SHAPED 8-PSK

BANDWIDTH EFFICIENCY

AND SPECTRAL SPIKE ELIMINATION

JIANPING TAO, B.EBG.

NMSU-ECE-98-003 MAY 1998

Presented to Dr. James LeBlanc

in partial fulfillment of the requirements

for the Degree

Master of Science in Electrical Engineering

New Mexico State University

Las Cruces, New Mexico

May 1998

ACKNOWLEDGMENTS

I would like to thank Dr. James P. LeBlanc, my advisor, for his help and direction in the development and preparation of this report. I am truly indebted to Dr. Sheila B. Horan who brought me to the communication field, for her advice, help and direction in my research. I also wish to thank Dr. Phillip De Leon for his direction on the sampling theorem and advice in my report. I thank Dr. Tonghui Wang for his valuable advice in my report. I am grateful to Dr. Marvin K. Simon at the Jet Propulsion Laboratory, for providing me his report on discrete spectrum.

I would like to thank the National Aeronautics and Space Administration (NASA) for their support under Grant NASA# NAG 5-1491 and for giving me the chance to work on this project. Also a special thank you to the people in the Center for Space Telemetry and Telecommunications Systems at New Mexico State University for their assistance.

ABSTRACT

PULSE SHAPED 8-PSK

BANDWIDTH EFFICIENCY

AND SPECTRAL SPIKE ELIMINATION

BY

JIANPING TAO, B.EBG.

Master of Science in Electrical Engineering

New Mexico State University

Las Cruces, New Mexico, 1998

Dr. James P. LeBlanc, Chair

The most bandwidth-efficient communication methods are imperative to cope with the congested frequency bands. Pulse shaping methods have excellent effects on narrowing bandwidth and increasing band utilization. The position of the baseband filters for the pulse shaping is crucial. Post-modulation pulse shaping (a low pass filter is located after the modulator) can change signals from constant envelope to non-constant envelope, and non-constant envelope signals through non-linear device (a SSPA or TWT) can further spread the power spectra [6]. Pre-modulation pulse

shaping (a filter is located before the modulator) will have constant envelope. These two pulse shaping methods have different effects on narrowing the bandwidth and producing bit errors. This report studied the effect of various pre-modulation pulse shaping filters with respect to bandwidth, spectral spikes and bit error rate. A pre-modulation pulse shaped 8-ary Phase Shift Keying (8PSK) modulation was used throughout the simulations.

In addition to traditional pulse shaping filters, such as Bessel, Butterworth and Square Root Raised Cosine (SRRC), other kinds of filters or pulse waveforms were also studied in the pre-modulation pulse shaping method. Simulations were conducted by using the Signal Processing Worksystem (SPW) software package on HP workstations which simulated the power spectral density of pulse shaped 8-PSK signals, end to end system performance and bit error rates (BERs) as a function of Eb/No using pulse shaping in an AWGN channel. These results are compared with the post-modulation pulse shaped 8-PSK results.

The simulations indicate traditional pulse shaping filters used in pre-modulation pulse shaping may produce narrower bandwidth, but with worse BER than those in post-modulation pulse shaping. Theory and simulations show pre-modulation pulse shaping could also produce discrete line power spectra (spikes) at regular frequency intervals. These spikes may cause interference with adjacent channel and reduce power efficiency. Some particular pulses (filters), such as trapezoid and pulses with different transits (such as weighted raised cosine transit)

were found to reduce bandwidth and not generate spectral spikes. Although a solid state power amplifier (SSPA) was simulated in the non-linear (saturation) region, output power spectra did not spread due to the constant envelope 8-PSK signals.

TABLE OF CONTENTS

LIST OF TABLES

LIST OF FIGURES

LIST OF ABBREVIATIONS

α	Rolloff Factor for SRRC filters
ρ	Band Utilization Ratio
AWGN	Additive White Gaussian Noise
dB	Decibels
BER	Bit Error Rate
BPSK	Binary Phase Shift Keying
BW	Bandwidth
BT	Bandwidth-Time (symbol) product
CCSDS	Consultative Committee for Space Data Systems
Eb/No	Energy (bit) to Noise ratio
ESA	European Space Agency
f_s	Sampling Frequency
f_c	Carrier Frequency
FFT	Fast Fourier Transform
Hz	Hertz
HP	Hewlett Packard
IIR	Infinite Impulse Response (Filter)
ISI	Intersymbol Interference
JPL	Jet Propulsion Laboratory
LSB	Least Significant Bit
MSB	Most Significant Bit
MSK	Minimum Shift Keying
NASA	National Aeronautics and Space Administration
NMSU	New Mexico State University
NRZ-L	Non-Return-to-Zero Logic
QPSK	Quaternary Phase Shift Keying

PA	Power Amplifier
PCM	Pulse Coded Modulation
PM	Phase Modulation
PSD	Power Spectral Density
PSK	Phase Shift Keying
QPSK	Quartenary Phase Shift Keying
R_b	Bit Rate
R_S	Symbol or Baud Rate
RC	Raised Cosine
sec	Seconds
SFCG	Space Frequency Coordination Group
SNR	Signal-to-Noise Ratio
SPW	Signal Processing Worksystem
SSPA	Solid State Power Amplifier
SRRC	Square Root Raised Cosine
T_b	Bit Period
TWT	Traveling Wave Tube

Chapter 1

INTRODUCTION

With the continuing development of communications and increasing users, frequency bands are becoming more and more congested. In order to cope with this frequency congestion, methods to increase bandwidth utilization have be studied in [1]~[6] and [13]~[16]. These methods consider efficient modulation which is implemented using pulse shaping methods.

Two kinds of pulse shaping methods have been investigated to realize bandwidth efficiency. One kind of pulse shaping methods is pre-modulation pulse shaping which performs a low pass filtering before modulation to reduce bandwidth. Pre-modulation pulse shaping with different modulation schemes, such Pulse Code Modulation (PCM), Binary Phase Shift Keying (BPSK), Quaternary Phase Shift Keying (QPSK) and Gaussian filtered Minimum Shift Keying (GMSK) have been studied in [13]~[16]. The other pulse shaping method is post-modulation pulse shaping which conducts low pass filtering after modulation. Caballero [6] has used this method to simulate 8 level Phase Shift Keying (8-PSK) signaling over non-linear satellite channels.

In [6] post-modulation pulse shaping method is investigated with various filters. Three kind of filters, consisting of a fifth order Butterworth, third order Bessel and Square Root Raised Cosine (SRRC) filters, with different Bandwidth-Time (BT)

product or roll off factor, have been used to reduce bandwidth in the simulations of 8-PSK over non-linear satellite channels. Because of post-modulation pulse shaping, it produced a non-constant envelope pulse shaped 8-PSK which can spread the power spectrum when the signals go through a non-linear Solid State Power Amplifier (SSPA). The simulations also included measures of symbol error rate (SER) for post-modulation pulse shaped 8-PSK signaling. Simulation results indicated that there is trade-off between bandwidth efficiency and SER.

Prabhu and Rowe [1] presented a matrix method for computing the power spectrum of digital phase modulation in 1974, and studied pre-modulation pulse shaped pulse train with or without overlapping. Pre-pulse shaping may produce not only a continuous component but also a discrete line component at some particular frequencies in power spectral density (PSD). Based on Prabhu and Rowe, Simon recently obtained explicit expressions for power spectrum when signaling is m-ary PSK in the presence of intersymbol interference (ISI) produced by pulse shaping.

Martin and Nguyen in [13],[15] and [16], Otter in [14] have studied different traditional filters (Butterworth, Bessel and SRRC filters) used as pre-pulse shaping for different modulation types (PCM, BPSK, QPSK and GMSK). By comparing pre-modulation pulse shaping and post-modulation pulse shaping, Martin and Nguyen indicated that pre-modulation pulse shaping can overcome disadvantages produced by post modulation pulse shaping, such as larger, heavy filters which are not compatible with some mission operations requirements.

In contrast to using traditional filters by Martin and Nguyen, Greenstein [4] has examined PSK with different overlapping baseband pulses. Greenstein investigated triangular, cosine, raised cosine and Nyquest pulse shapes, yielding the results for continuous and discrete line components of PSD.

Although many studies have investigated pre-modulation pulse shaping and post-modulation pulse shaping with various filters, post-modulation pulse shaping can induce a non-constant envelope signaling which can spread the reduced bandwidth. Pre-modulation pulse shaping can induce power spectral spikes which are not good for power efficiency and may produce adjacent channel interference. A study is needed for pre-modulation pulse shaping which produces a constant modules signal with no spikes

This project conducted simulations on pre-pulse shaped 8-PSK over non-linear channel. First, three kinds of traditional filters, 5th order Butterworth, 3rd order Bessel and SRRC, were used as pulse shaping filter applied to 8-PSK phase signals. Filtered phase signals were then modulated to become pulse shaped 8-PSK signals. Pulse shaped 8-PSK signals were amplified by a non-linear SSPA. In order to simulate channel noise, an additive white Gaussian noise (AWGN) was added. At the receiver, an integrate and dump circuit was used. Power spectra produced by pre-modulation pulse shaping were compared with those using post-modulation pulse shaping. In addition, received bit error rate (BER) was also compared between two pulse shaping methods. Second, theoretical power spectrum for pulse shaped 8-PSK

was studied based on [1] and [2]. Third, many pulse waveforms were found for 8-PSK to reduce bandwidth and reduce or eliminate power spectral spikes. Simulations and numerical results indicated that trapezoid and weighted raised cosine transit pulses with more than two symbol periods can get rid of spectral spikes. These results are in agreement with Simon's recent report [3]. Finally, According to simulation results, recommendations were given for searching for optimal pulses to reduce bandwidth without spikes.

Chapter 2

THEORY

This section will introduce some of the concepts which were used for this project. First, 8-PSK signals and pulse shaping methods will be described. Butterworth, Bessel and Raised Cosine Filters are discussed as traditional pulse shaping filters. Second, a detailed discussion of pulse shaping waveforms and power spectral components of pre-modulation pulse shaped PSK signals will be presented. Pre-modulation pulse shaped 8-PSK power spectra consist of continuous and discrete line (spikes) components. Various pulse shaping waveforms, such as trapezoid and raised cosine are used. Third, since a Solid State Power Amplifier (SSPA) was used in the simulations, the characteristics of the SSPA will be studied. Finally, the topic will be an Additive White Gaussian Noise (AWGN) channel and a matched filter used as receiver.

2.1 8-PSK Pulse Shaping Methods

In 8 level Phase-Shift Keying (8-PSK), information is contained in the phase of the signal, and each symbol has 3 bits. The phase of the carrier can take one of 8 equally-spaced values, such as in Table 2-1 and shown in Figure 2-1. A plot of 8PSK signal constellation is shown in Figure 2-1. An 8-PSK signal, S(t), can be expressed as following.

$$S(t) = A_c\exp[j(\omega_c t + \varphi(t))] = A_c\cos[\omega_c t + \varphi(t)] + jA_c\sin[\omega_c t + \varphi(t)] \qquad (2\text{-}1)$$

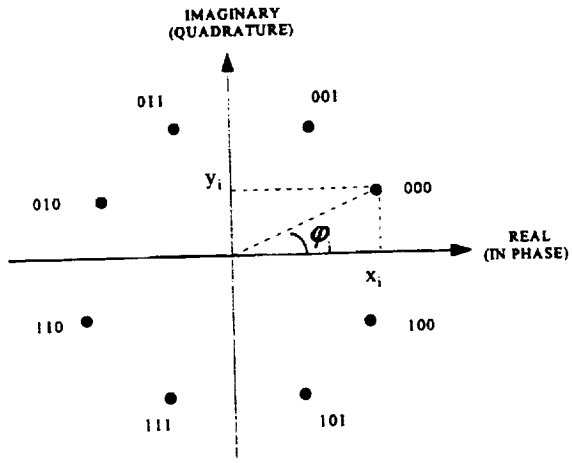

Figure 2-1 8PSK Signal Constellation

Where the envelope A_c is constant in this project, $\omega_c = 2\pi f_c$, and f_c is the carrier frequency in hertz, φ is the phase which takes on one of the 8 discrete values (in degrees) corresponding to the 3 bit Gray code. Table 2-1 shows the relationship between Gray codes and φ.

Table 2-1 Gray Codes and Phase φ

Binary Gray Codes	φ (Degree)
000	22.5^o
001	67.5^o
011	112.5^o
010	157.5^o
110	147.5^o
111	247.5^o
101	292.5^o
100	337.5^o

In SPW, the Gray codes and phase φ can be produced by the design shown in Figure 2-2.

The phase signals $\varphi(t)$ can be modulated to 8-PSK signals v(t), where $v(t)=A_c e^{j\varphi(t)}$. To realize the pre-modulation pulse shaping, the phase signal, $\varphi(t)$, goes through a pulse shaping filter before it is modulated. In this project, various filters are used. In addition, the change of the position of the pulse shaping filters can produce a change in results. If the pulse shaping filter is placed after the modulator [5], this method is called as post-modulation pulse shaping. Figure 2-3 shows the modulation for unfiltered and filtered 8-PSK signals.

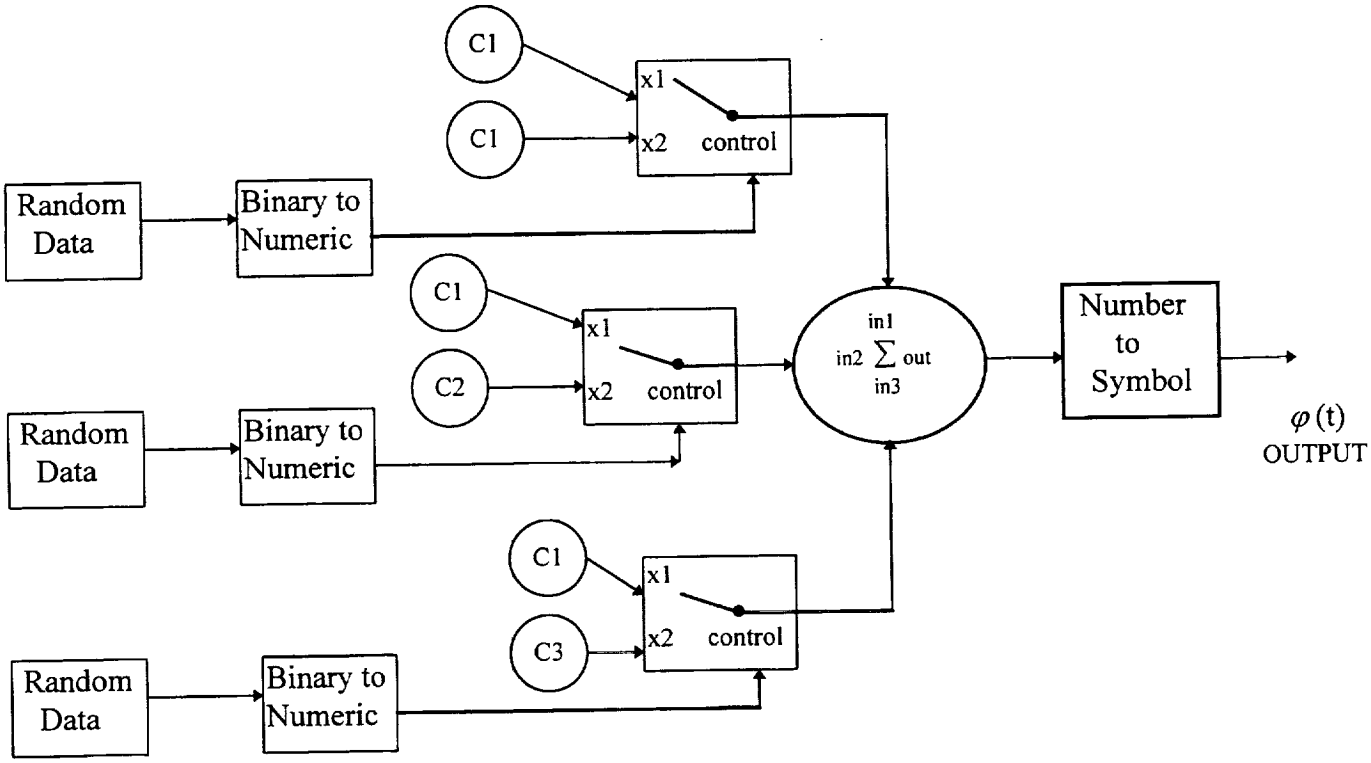

Figure 2-2 Producing Phase Signals Block Diagram
Where C1=1, C2=2, and C3=4. The Number to Symbol block functions as Table 2-1, and completes the conversion from Gray codes to phase in degrees.

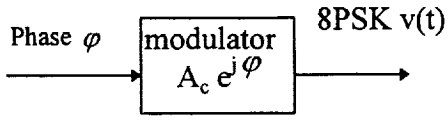

(a) Unfiltered 8PSK With Constant Envelope

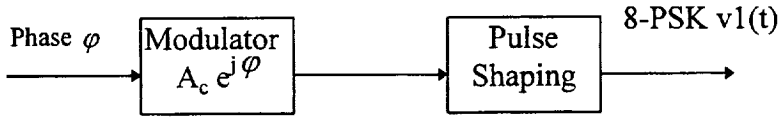

(b) Post-Modulation Pulse Shaping Method

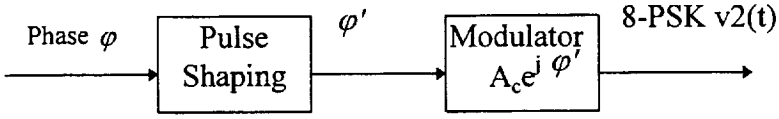

(c) Pre-Modulation Pulse Shaping Method

Figure 2-3. Modulation Schemes for Unfiltered and Filtered Phase Signals.

2.2 Filters Used for 8-PSK Pulse Shaping

Pulse Shaping Filters are used to narrow bandwidth and improve bandwidth utilization. In this report several traditional types of filters such as the 5th order Butterworth, 3rd-order Bessel and Square Root Raised Cosine (SRRC)(α=1) are utilized in the simulations. Other kinds of filters with overlapping or non-overlapping pulses, will be introduced in section 2.3.2.

Pulse shaping can induce distortions of 8-PSK signals and increase the risk of Inter-Symbol Interference (ISI)[4]. The distortions due to the pulse shaping filters make the implementation of an optimal receiver difficult.

Butterworth filters: Butterworth filters provide the maximally flat response in the passband. Response varies monotonically within the stopband, decreasing smoothly from $\Omega=0$ and $\Omega=\infty$. In the simulations, the 5th order Butterworth filter was used. The Figure 2-4 shows the amplitude response for different orders of Butterworth filters. The cut off frequency f_c corresponds to -3dB amplitude point.

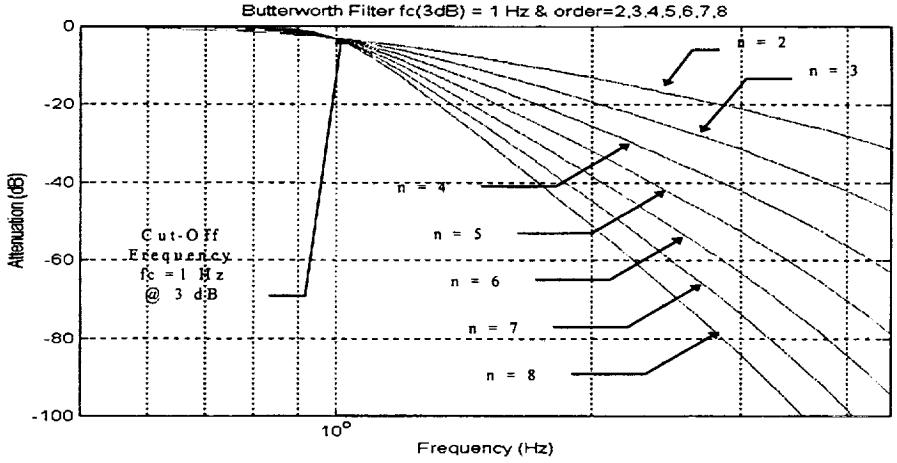

Figure 2-4 Amplitude Response of Various Orders of Butterworth Filters

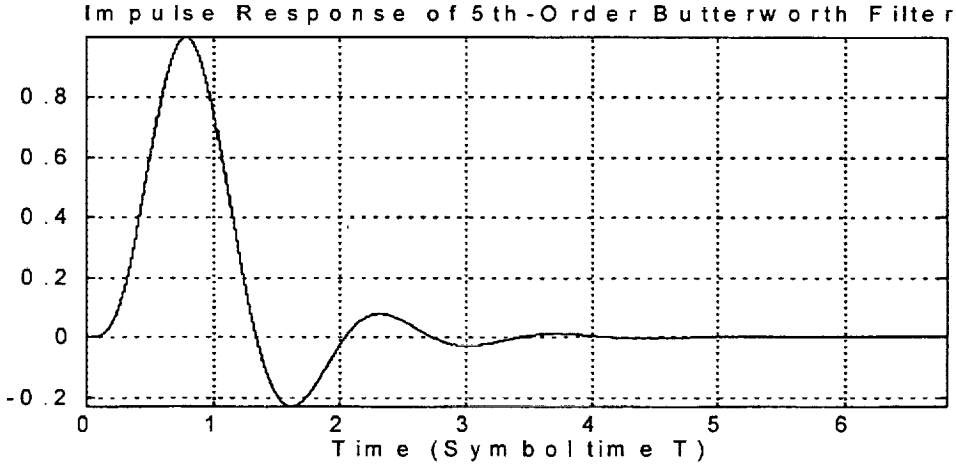

Figure 2-5 An Impulse Response of 5th-Order of Butterworth Filter

All orders of this filter pass through the 3 dB cut-off point. An impulse response of 5-order Butterwouth filter is shown in Figure 2-5. Since the duration of the impulse response is more than one symbol period T, it may produce Intersymbol Interference (ISI).

Bessel Filters: The Bessel type of filter has the slowest transition between passband and stopband and the passband phase response is better than the Butterworth. It has approximately linear phase in the passband so that it has a property of preventing dispersion of the signal. The amplitude for Bessel filters is not as flat in the passband region as for the Butterworth filters. This project uses a 3rd order Bessel filter for the simulation. Figure 2-6 shows the amplitude response of various orders of Bessel Filters. Note that the amplitude is not as flat in the passband region as for the Butterworth filter.

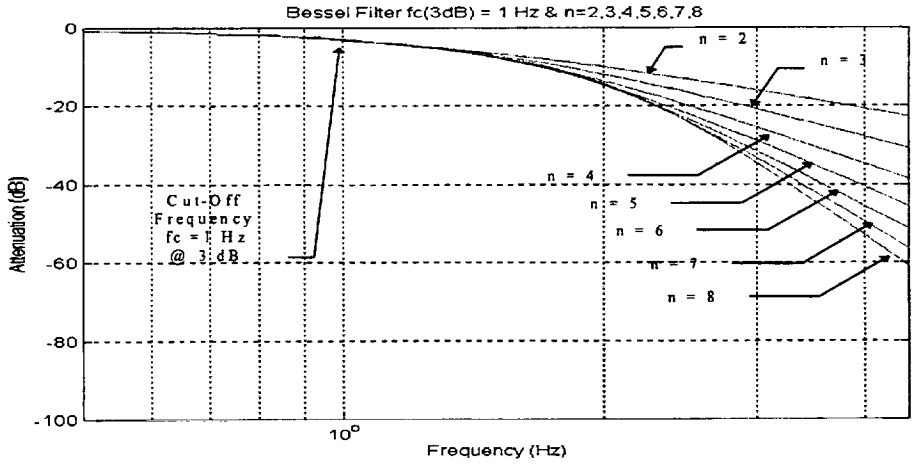

Figure 2-6 Amplitude Response of Various Orders of Bessel Filters

Also the transition from the passband to the stopband region is not as rapid as for the Butterworth Filters for the various orders of filters. An impulse response of the 3-order Buessel filter is shown in Figure 2-7.

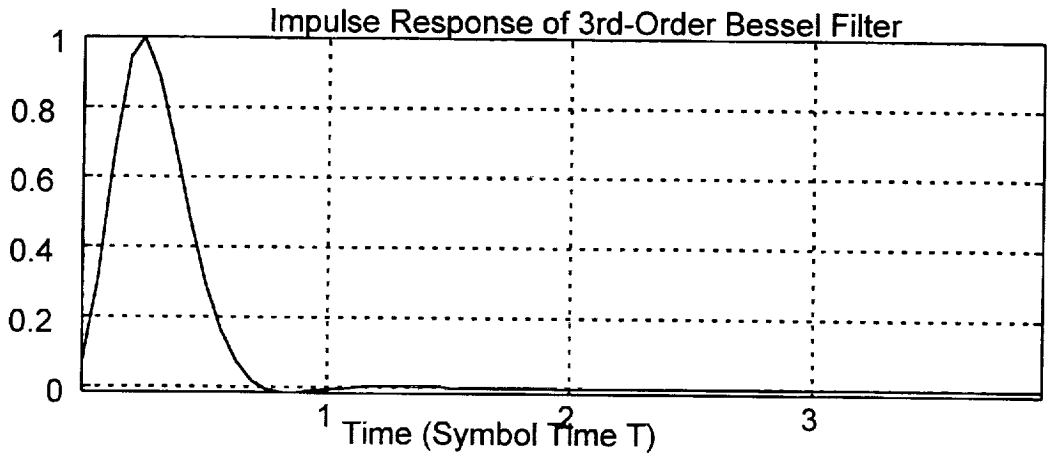

Figure 2-7 An Impulse Response of 3rd-Order of Bessel Filter

Square Root Raised Cosine Filter (α=1) The Raised Cosine filters are used to eliminate ISI in a linear channel. The transfer function of the Raised Cosine Filter is

$$RC(f)=\begin{cases} T, & 0 \le |f| < \dfrac{(1-\alpha)}{2T} \\ \dfrac{T}{2}\left(1-\sin\left[\dfrac{(2\pi|f|T-\pi)}{2\alpha}\right]\right), & \dfrac{(1-\alpha)}{2T} \le |f| \le \dfrac{(1+\alpha)}{2T} \\ 0, & |f| > \dfrac{(1+\alpha)}{2T} \end{cases} \qquad (2\text{-}2)$$

where the zeros will occur at t = nT (T is the sampling interval) and α is the rolloff factor or the excess bandwidth over the Nyquist Band Filter which can be varied from 0 to 1. The rolloff factor, α, determines the bandwidth of a Raised Cosine Filter. Figure 2-8 shows the

frequency response of the Raised Cosine Function with different rolloff factors ($\alpha = 0$, 0.25, 0.5 and 1) and T =1 seconds.

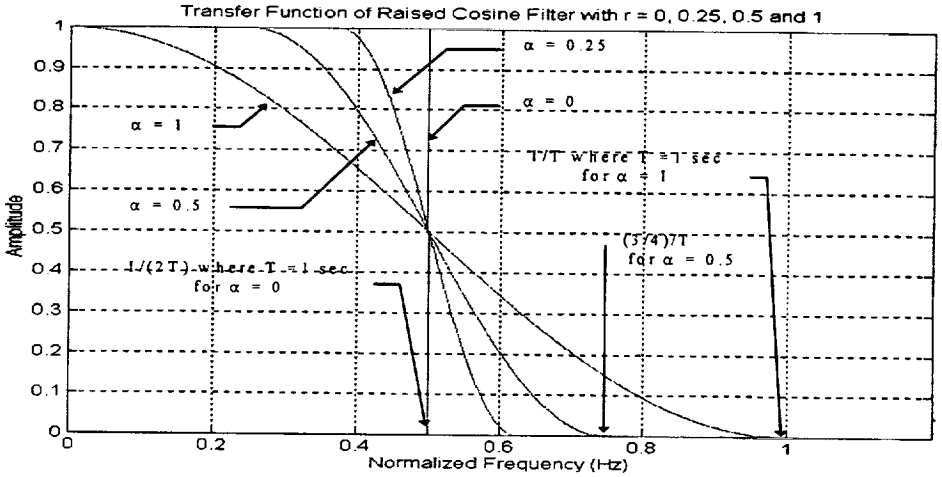

Figure 2-8 Frequency Response: Raised Cosine Characteristics with Different α

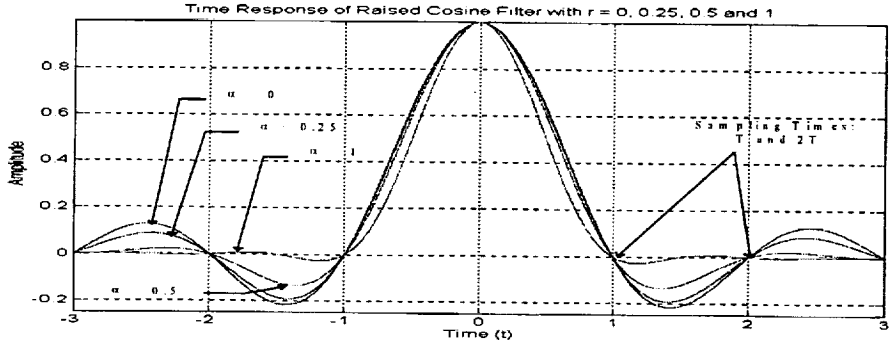

Figure 2-9 Impulse Response of Raised Cosine Filters for Different α

Figure 2-9 gives impulse response for different rolloff factors. From Figure 2-9, it can be seen that if the symbols are sampled at the nulls of the sinc function then the symbol interference from the previous and next symbols will not exist. As mentioned in [17], if the Raised cosine filters are used the ISI will be eliminated in a linear channel. To eliminate ISI in a linear channel, a Square Root Raised Cosine filter is used in both the

transmitter and the receiver. If RC(f) is the frequency response of the Raised Cosine Filter, the frequency response of Square Root Raised Cosine filter is

$$SRRC(f)=\sqrt{RC(f)} \tag{2-3}$$

According to [10], the coefficients of SRRC filter can be obtained from the formula (2-4):

$$h(t)=4\ \alpha\ \frac{[\cos((1+\alpha)\pi\frac{t}{T})+\sin((1-\alpha)\pi\frac{t}{T})]}{\pi\sqrt{T}[(4\alpha\frac{t}{T})^{2}-1]} \tag{2-4}$$

In this equation, α is the roll off parameter and T is one symbol period (1/symbol rate). The Real Raised cosine block in SPW is selected for the project simulation. Ture SRRC filtering is noncausal and has infinite coefficients, but actually a finite number of coefficients are needed to determine the FIR tap length. This truncation can cause some frequency distortion. Since pre-modulation pulse shaping makes the channel no longer linear, simulation will show that SRRC can not eliminate ISI.

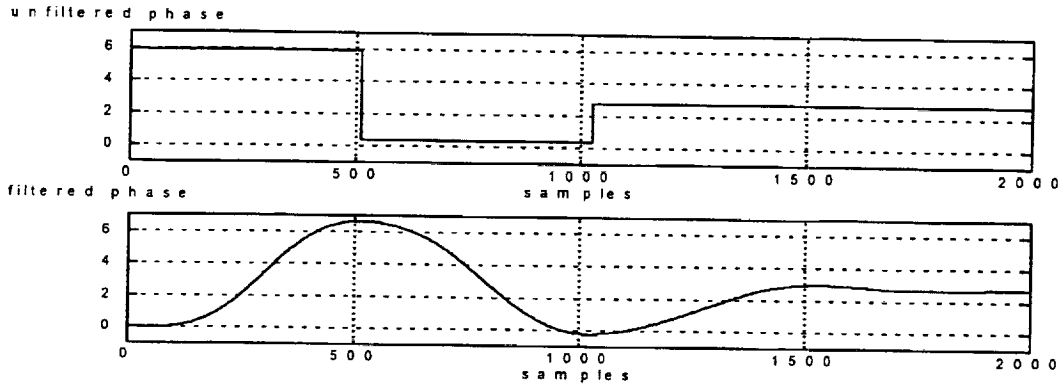

Figure 2-10 The Waveforms of Phase φ and Filtered Phase φ'
(Butterworth 5th filter is used, BT=1)

The Observation of Pulse Shaped 8-PSK Waveforms. With the use of pulse shaping filters, the 8-PSK signals change their shapes. The main character of the waveform change

is a transient (rise and drop) in the filtered φ' (as shown in Figure 2-10). In Figure 2-10, it can be seen that the filtered phase φ' has a smooth transition from 0 to 2π, in sample range 0 to 500. The transient (rise or drop) makes the big difference between unfiltered and the filtered 8-PSK shown in Figure 2-11 and Figure 2-12.

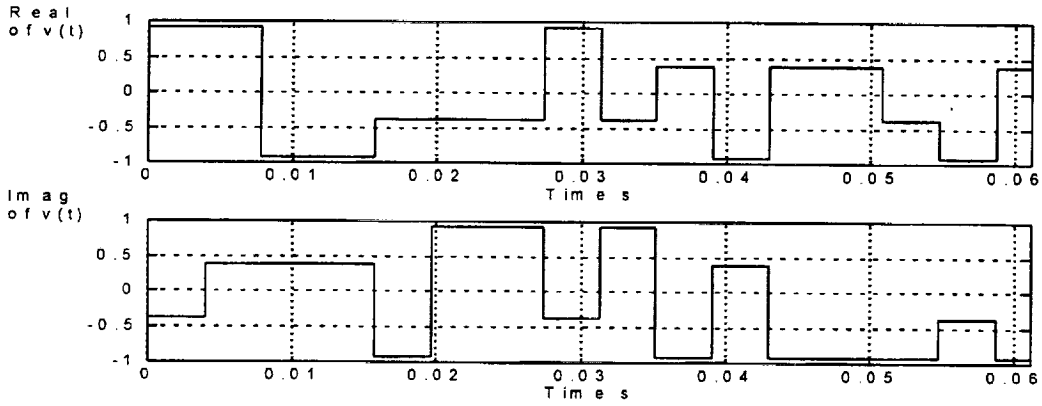

Figure 2-11 The Waveforms of Real Part and Imaginary Part of 8-PSK

The filtering process elongates data symbols such that they overlap one another. This shows the existence of Intersymbol Interference (ISI) introduced by the filtering process. When the pulse waveforms pass through the bandlimited system, they will be spread or dispersed which increases error rates and affects power spectrum.

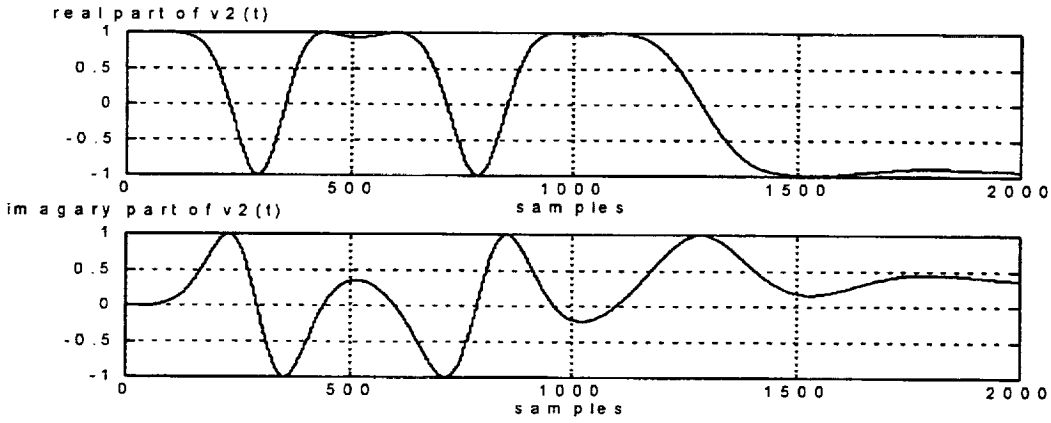

Figure 2-12 The Waveforms of Real Part and Imaginary Part of Pre-Modulation Filtered 8-PSK (512 Samples/Symbol)

2. 3 Power Spectral Components and Pulse Shaping Waveforms

Pre-modulation pulse shaping for phase modulation could produce power spectra with not only continuous components but also spikes [1]-[4] and [13]-[16]. Prabhu and Rowe [1] have given a rigorous discussion for components of pulse shaped PSK power spectra. Simon [2] & [3] have also derived explicit formulas for continuous and discrete components of pulse shaped PSK based on [1]. Greenstein [4] studied numerous pulse shapes and compared their efficiency of narrowing bandwidth. In this section, 8-PSK power spectral components based on [1] and [2] with an assumption of cyclostationary will be discussed.

2. 3.1 Baseband Pulse Shaped 8-PSK Vector-Matrix Notation

The following developments on power spectra of pre-modulation pulse shaped 8-PSK are based on [1]. A digital angle-modulated carrier of the form can be described as

$$s(t)= \cos [2\pi f_c t+\varphi(t)]$$

$$=\mathrm{Re}\{\exp[j2\pi f_c t+\varphi(t)]\}, \qquad (2\text{-}5)$$

where $\varphi(t)$ is a digital angle modulation, and f_c is the carrier frequency. For convenience, define the equivalent complex baseband modulation

$$v(t)=\exp(j\varphi(t)), \qquad (2\text{-}6)$$

According to Prabhu and Rowe, the spectrum of s(t) is

$$P_s(f)=\frac{1}{4}P_v(f-f_c)+\frac{1}{4}P_v(-f-f_c), \qquad (2\text{-}7)$$

where P_v is the spectrum of v(t).

For pre-modulation pulse shaped 8-PSK, $\varphi(t)$ takes on one of eight level pulses.

$$g_i(t)=\frac{\pi}{8}\,[8-(2i-1)]p(t)\,, \qquad (i=1,2....8) \qquad (2\text{-}8)$$

Where p(t) is the pulse shaped waveform which may be the result of a rectangular pulse passed through an ISI-producing filter. Denote a column vector **g(t)** such that

$$\mathbf{g(t)} =[g_1(t)\ g_2(t)\ g_3(t)\ g_4(t)\ g_5(t)\ g_6(t)\ g_7(t)\ g_8(t)]^T\,. \qquad (2\text{-}9)$$

If $g_i(t)$ is strictly time-limited to a bit interval T, for example, let i=2, then

$$\varphi(t) =g_2(t)=\frac{\pi}{8}\,5p(t). \quad ;0\le t\le T \qquad (2\text{-}10)$$

Using vector notation, $\varphi(t)$ becomes

$$\varphi(t) =[0\ 1\ 0\ 0\ 0\ 0\ 0\ 0]\mathbf{g(t)} \qquad (2\text{-}11)$$

For convenience, a column $\mathbf{a}_k$ vector is defined as:

$$\mathbf{a}_k =[\,a_k^{(1)}\ a_k^{(2)}\ a_k^{(3)}\ a_k^{(4)}\ a_k^{(5)}\ a_k^{(6)}\ a_k^{(7)}\ a_k^{(8)}]^T,$$

and define the basis column vector

$$\mathbf{e}_1=[1\ 0\ 0\ 0\ 0\ 0\ 0\ 0]^T$$

$$\mathbf{e}_2=[0\ 1\ 0\ 0\ 0\ 0\ 0\ 0]^T$$

$$\vdots$$

$$\mathbf{e}_8=[0\ 0\ 0\ 0\ 0\ 0\ 0\ 1]^T \qquad (2\text{-}12)$$

and $\mathbf{a}_k$ takes on only one of the values $\mathbf{e}_1$, $\mathbf{e}_2$, ... $\mathbf{e}_8$ with the same probability $\frac{1}{8}$, then $\varphi(t)$ may be expressed as

$$\varphi(t)=\sum_{k=-\infty}^{\infty} \mathbf{a}_k^T \mathbf{g(t)} \qquad ; -\infty \le t \le \infty \qquad (2\text{-}13)$$

Using the same idea, define two vectors $\mathbf{b}_k$ and $\mathbf{r(t)}$, such that

$$\mathbf{b}_k=[\,b_k^{(1)}\ b_k^{(2)}\ b_k^{(3)}\ b_k^{(4)}\ b_k^{(5)}\ b_k^{(6)}\ b_k^{(7)}\ b_k^{(8)}]^T, \qquad (2\text{-}14)$$

$\mathbf{b}_k$ also takes on only one of the values $\mathbf{e}_1$, $\mathbf{e}_2$, ... $\mathbf{e}_8$ with the same probability $\frac{1}{8}$,

$$\mathbf{r\ (t)}=\exp[j\mathbf{g(t)}]=[\,\exp(jg_1(t))\ \exp(jg_2(t))\ ...\ \exp(jg_8(t))\,]^T. \qquad (2\text{-}15)$$

According to (2-10), the complex baseband 8-PSK modulation may be described as

$$v(t)=\exp[j\varphi(t)]=\exp[jg_2(t)]=\exp[j\frac{\pi}{8}\ 5p(t)] \quad ; 0 \le t \le T \qquad (2\text{-}16)$$

$$=[0\ 1\ 0\ 0\ 0\ 0\ 0\ 0]\mathbf{r\ (t)}\ =\mathbf{b}_2^T\ \mathbf{r(t)} \qquad ; 0 \le t \le T \qquad (2\text{-}17)$$

Then v(t) can be written as

$$v(t)=\sum_{k=-\infty}^{\infty} \mathbf{b}_k^T \mathbf{r}(t-kT) \qquad ; -\infty \le t \le \infty \tag{2-18}$$

2. 3.2 Power Spectral Components of Pulse Shaped 8-PSK

In order to determine the spectral density of (2-18), the signal $\mathbf{r}(t)$ is deterministic, and $\mathbf{b}_k$ is a random vector sequence from 2-14. Assume that $\mathbf{b}_k$ is wide-sense stationary. Then, define a mean vector $\mathbf{M}_b$ of $\mathbf{b}_k$ as follows

$$\mathbf{M}_b=E[\mathbf{b}_k] . \tag{2-19}$$

If all signal pulses are equally likely,

$$\mathbf{M}_b =\frac{1}{8} [1\ 1\ 1\ 1\ 1\ 1\ 1\ 1\ ]^T . \tag{2-20}$$

The autocorrelation function matrix of $\mathbf{b}_k$ is

$$\overline{\overline{R_b}}\ (k-l)=E[\mathbf{b}_k\, \mathbf{b}_l^H], \tag{2-21}$$

and the power spectral density matrix of $\mathbf{b}_k$ is

$$\overline{\overline{P_b}}(f)= \sum_{n=-\infty}^{\infty} e^{-j2\pi fn} \overline{\overline{R_b}}\ (n). \tag{2-22}$$

The goal is to find the power spectral density of the baseband 8-PSK signal v(t). The autocorrelation function of v(t) is given by

$$R_v(t+\tau ,t) = E[v(t+\tau)v^*(t)] \tag{2-23}$$

$$=E\Big\{ \sum_{k=-\infty}^{\infty} \mathbf{b}_k^T \mathbf{r}(t+\tau -kT)[\sum_{l=-\infty}^{\infty} \mathbf{b}_k^T \mathbf{r}(t-lT)]^* \Big\}$$

$$=E\Big[\sum_{k=-\infty}^{\infty} \mathbf{b}_k^T \mathbf{r}(t+\tau -kT) \sum_{l=-\infty}^{\infty} \mathbf{b}_l^H \mathbf{r}^*(t-lT)\Big]$$

$$=E\Big[\sum_{k=-\infty}^{\infty}\sum_{l=-\infty}^{\infty}\mathbf{b}_k^{T}\mathbf{r}(t+\tau-kT)\,\mathbf{b}_l^{H}\mathbf{r}^{*}(t-lT)\Big]$$

$$=E\Big[\sum_{k=-\infty}^{\infty}\sum_{l=-\infty}^{\infty}\mathbf{r}^{T}(t+\tau-kT)\,\mathbf{b}_k\mathbf{b}_l^{H}\mathbf{r}^{*}(t-lT)\Big]$$

$$=\sum_{k=-\infty}^{\infty}\sum_{l=-\infty}^{\infty}\mathbf{r}^{T}(t+\tau-kT)\,E\Big[\mathbf{b}_k\mathbf{b}_l^{H}\Big]\,\mathbf{r}^{*}(t-lT)\Big]$$

$$=\sum_{k=-\infty}^{\infty}\sum_{l=-\infty}^{\infty}\mathbf{r}^{T}(t+\tau-kT)\,\overline{\overline{R}}_b(k-l)\mathbf{r}^{*}(t-lT) \qquad (2\text{-}24)$$

From (2-24), it is easy to show

$$R_v(t+nT+\tau,t+nT)=R_v(t+\tau,t), \qquad (2\text{-}25)$$

then, v(t) is cyclostationary. According to [9], the time-average autocorrelation function over a signal period is defined as

$$R_v(\tau)=\frac{1}{T}\int_{-\frac{T}{2}}^{\frac{T}{2}}R_v(t+\tau,t)\,dt \qquad (2\text{-}26)$$

Substituting (2-24) in (2-26),

$$R_v(\tau)=\frac{1}{T}\sum_{k=-\infty}^{\infty}\sum_{l=-\infty}^{\infty}\int_{-\frac{T}{2}}^{\frac{T}{2}}\mathbf{r}^{T}(t+\tau-kT)\,\overline{\overline{R}}_b(k-l)\mathbf{r}^{*}(t-lT)\,dt.$$

Let k-l=n and t-lT =x,

$$R_v(\tau)=\frac{1}{T}\sum_{n=-\infty}^{\infty}\sum_{l=-\infty}^{\infty}\int_{-\frac{T}{2}-lT}^{\frac{T}{2}-lT}\mathbf{r}^{T}(t+\tau-nT)\,\overline{\overline{R}}_b(n)\mathbf{r}^{*}(x)dx$$

$$= \frac{1}{T} \sum_{n=-\infty}^{\infty} \int_{-\infty}^{\infty} \mathbf{r}^T(t+\tau-nT)\, \overline{\overline{R_b}}(n)\mathbf{r}^*(x)dx$$

Let t=x, then

$$R_v(\tau) = \frac{1}{T} \sum_{n=-\infty}^{\infty} \int_{-\infty}^{\infty} \mathbf{r}^T(t+\tau-nT)\, \overline{\overline{R_b}}(n)\mathbf{r}^*(t)dt \qquad (2\text{-}27)$$

Power spectral density of v(t) is defined as

$$P_v(f) = \int_{-\infty}^{\infty} R_v(\tau) e^{-j2\pi f \tau}\, d\tau \qquad (2\text{-}28)$$

$$= \int_{-\infty}^{\infty} \frac{1}{T} \sum_{n=-\infty}^{\infty} \int_{-\infty}^{\infty} e^{-j2\pi f \tau}\, \mathbf{r}^T(t+\tau-nT)\, \overline{\overline{R_b}}(n)\mathbf{r}^*(t)dt\, d\tau$$

$$= \frac{1}{T} \sum_{n=-\infty}^{\infty} \int_{-\infty}^{\infty} \int_{-\infty}^{\infty} e^{-j2\pi f \tau}\, \mathbf{r}^T(t+\tau-nT)\, \overline{\overline{R_b}}(n)\mathbf{r}^*(t)\, dt\, d\tau .$$

Let x= t+ τ , then

$$P_v(f) = \frac{1}{T} \sum_{n=-\infty}^{\infty} \int_{-\infty}^{\infty} e^{-j2\pi fx}\, \mathbf{r}^T(x-nT)\overline{\overline{R_b}}(n)\, dx \int_{-\infty}^{\infty} e^{j2\pi f \tau}\, \mathbf{r}^*(t)\, dt\, d\tau .$$

$\mathbf{R}(f) = \int_{-\infty}^{\infty} e^{-j2\pi ft}\mathbf{r}(t)\, dt$, is the Fourier transform of $\mathbf{r}(t)$, and it is also a column vector.

Thus $P_v(f)$ can be expressed as

$$P_v(f) = \frac{1}{T} \sum_{n=-\infty}^{\infty} \mathbf{R}^T(f)\, e^{-j2\pi fnT}\, \overline{\overline{R_b}}(n)\, \mathbf{R}^*(f)$$

$$= \frac{1}{T} \mathbf{R}^T(f) \{ \sum_{n=-\infty}^{\infty} e^{-j2\pi fnT}\, \overline{\overline{R_b}}(n) \} \mathbf{R}^*(f) \qquad (2\text{-}29)$$

By using (2-22), $P_v(f)$ becomes

$$P_v(f) = \frac{1}{T}\, \mathbf{R}^T(f)\, \overline{\overline{P_b}}(fT)\mathbf{R}^*(f) \qquad (2\text{-}30)$$

since

$$\overline{\overline{P_b}}(f) = \sum_{n=-\infty}^{\infty} e^{-j2\pi fn}\, \overline{\overline{R_b}}(n).$$

Introducing covariance matrix $\overline{\overline{K_b}}(n) = \overline{\overline{R_b}}(n) - \mathbf{M_b}\,\mathbf{M_b}^{\mathbf{H}}$, then

$$\overline{\overline{P_b}}(f) = \sum_{n=-\infty}^{\infty} e^{-j2\pi fn}(\overline{\overline{K_b}}(n) + \mathbf{M_b}\,\mathbf{M_b}^{\mathbf{H}})$$

$$= \sum_{n=-\infty}^{\infty} e^{-j2\pi fn}\, \overline{\overline{K_b}}(n) + \mathbf{M_b}\,\mathbf{M_b}^{\mathbf{H}} \sum_{n=-\infty}^{\infty} e^{-j2\pi fn}\,. \qquad (2\text{-}31)$$

Using Fourier series, we have

$$\sum_{n=-\infty}^{\infty} e^{-j2\pi fn} = \sum_{n=-\infty}^{\infty} \delta(f-n) \qquad (2\text{-}32)$$

$$\sum_{n=-\infty}^{\infty} e^{-j2\pi fTn} = \frac{1}{T} \sum_{n=-\infty}^{\infty} \delta\left(f-\frac{n}{T}\right)\,. \qquad (2\text{-}33)$$

Therefore,

$$\overline{\overline{P_b}}(f) = \sum_{n=-\infty}^{\infty} e^{-j2\pi fn}\, \overline{\overline{K_b}}(n) + \mathbf{M_b}\,\mathbf{M_b}^{\mathbf{H}} \sum_{n=-\infty}^{\infty} \delta(f-n)$$

$$= \overline{\overline{P_{bc}}}(f) + \overline{\overline{P_{bl}}}(f) \qquad (2\text{-}34)$$

where $\overline{\overline{P_{bc}}}(f)$ is continuous spectrum component, and $\overline{\overline{P_{bl}}}(f)$ is the discrete line spectrum component.

From (2-30) and (2-34),

$$P_v(f) = \frac{1}{T}\,\mathbf{R}^T(f)[\overline{\overline{P_{bc}}}(fT) + \overline{\overline{P_{bl}}}\,(fT)]\mathbf{R}^*(f)$$

$$= \frac{1}{T}\,\mathbf{R}^T(f)\,\overline{\overline{P_{bc}}}(fT)\,\mathbf{R}^*(f) + \frac{1}{T}\,\mathbf{R}^T(f)\,\overline{\overline{P_{bl}}}\,(fT)\mathbf{R}^*(f)$$

$$= P_{vc}(f) + P_{vl}(f) \qquad (2\text{-}35)$$

$P_{vc}(f)$ is the continuous component of the pulse shaped 8-PSK power spectral density. A further study on $P_{vl}(f)$ is given as follows.

$$P_{vl}(f) = \frac{1}{T}\,\mathbf{R}^T(f)\,\overline{\overline{P_{bl}}}\,(fT)\mathbf{R}^*(f)$$

$$= \frac{1}{T}\,\mathbf{R}^T(f)\{\,\frac{1}{T}\mathbf{M}_b\,\mathbf{M}_b^{H}\sum_{n=-\infty}^{\infty}\delta(f-\frac{n}{T})\}\mathbf{R}^*(f)$$

$$= \frac{1}{T^2}\,\mathbf{R}^T(f)\mathbf{M}_b\,\mathbf{M}_b^{H}\,\mathbf{R}^*(f)\sum_{n=-\infty}^{\infty}\delta(f-\frac{n}{T})$$

$$= \frac{1}{T^2}\,\mathbf{M}_b^{T}\,\mathbf{R}(f)\mathbf{M}_b^{H}\,\mathbf{R}^*(f)\sum_{n=-\infty}^{\infty}\delta(f-\frac{n}{T})$$

$$= \frac{1}{T^2}\,|\mathbf{M}_b^{T}\,\mathbf{R}(f)\,|^2\sum_{n=-\infty}^{\infty}\delta(f-\frac{n}{T})$$

$$= \frac{1}{T^2 8^2}\,|\sum_{i=1}^{8}\,R_i\,(f)\,|^2\sum_{n=-\infty}^{\infty}\delta(f-\frac{n}{T}). \qquad (2\text{-}36)$$

The $P_{vl}(f)$ is the discrete line component. (2-36) is the result of non-overlapping pulses, that is they are strictly time-limited to one symbol time. When signal pulses have overlapping, [1] defined a overlapping index K which stands for maximum signal pulse

duration. According to [1] and [2], $P_{vl}(f)$ for arbitrary index K may be expressed as

$$P_{vl}(f) = \frac{1}{T^2 8^{2K}} \left| \sum_{i=1}^{8^K} R_i(f) \right|^2 \sum_{n=-\infty}^{\infty} \delta(f - \frac{n}{T}). \qquad (2\text{-}37)$$

For 8-PSK with overlapping K=2, power spectral line component is

$$P_{vl}(f) = \frac{1}{T^2 8^4} \left| \sum_{i=1}^{8^2} R_i(f) \right|^2 \sum_{n=-\infty}^{\infty} \delta(f - \frac{n}{T}). \qquad (2\text{-}38)$$

and

$$\mathbf{R}(f) = \int_{-\infty}^{\infty} e^{-j2\pi ft} \mathbf{r}(t)\, dt$$

$$\mathbf{R}(f) = \int_0^T e^{-j2\pi ft} \begin{bmatrix} e^{j[\theta_1(t)+\theta_1(t-T)]} \\ \vdots \\ e^{j[\theta_1(t)+\theta_M(t-T)]} \\ e^{j[\theta_2(t)+\theta_1(t-T)]} \\ \vdots \\ e^{j[\theta_2(t)+\theta_M(t-T)]} \\ e^{j[\theta_3(t)+\theta_1(t-T)]} \\ \vdots \\ e^{j[\theta_{M-1}(t)+\theta_M(t-T)]} \\ e^{j[\theta_M(t)+\theta_1(t-T)]} \\ \vdots \\ e^{j[\theta_M(t)+\theta_M(t-T)]} \end{bmatrix} dt. \qquad (2\text{-}39)$$

where M=8 and $g_i(t)$ can be obtained from (2-8).

2. 3.3 Pulse Shaping Waveforms

Some particular signal pulses (filters) which overlap and do not overlap will be studied. According to [1], waveforms for different overlapping index K are shown as follows.

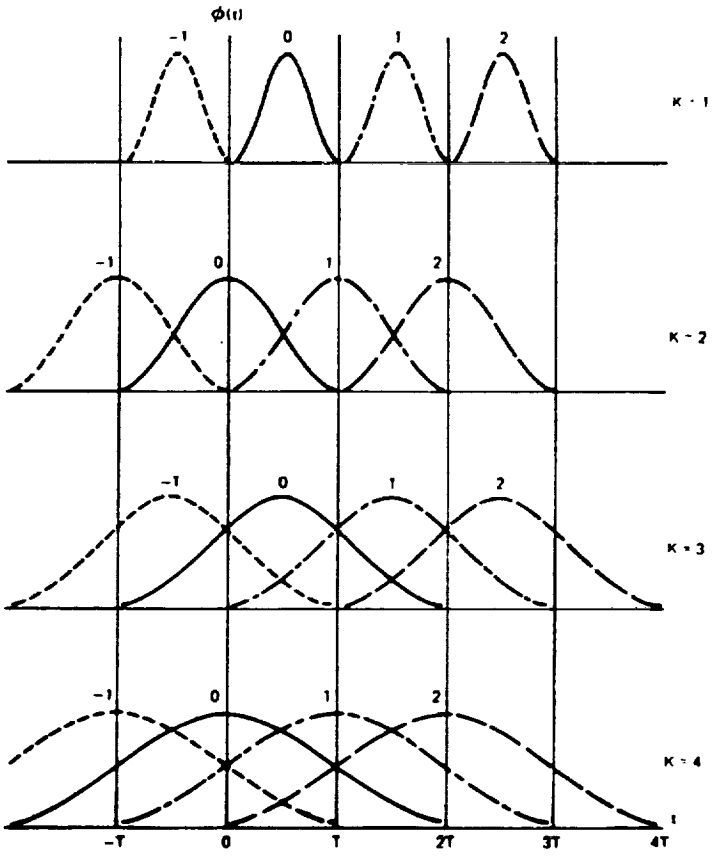

Figure 2-13 Pulses with different overlapping index K from [1]

Numerous pulse shapes with different pulse duration are simulated to investigate the effect on narrowing bandwidth and reducing spectral spikes. In the following expressions, T is used for one symbol time in seconds. In order to obtain a better effect on reducing spikes, some pulses will have T duration flat with different transits.

Cosine with Single-Interval T duration cosine with a single interval can be expressed as

$$p(t)=\begin{cases} \cos(\pi t/T) & |t| \le \dfrac{T}{2} \\ 0 & |t| > \dfrac{T}{2} \end{cases} \qquad (2\text{-}40)$$

T duration cosine pulse shaped and non-pulse shaped 8-PSK phase signals are shown in Figure 2-14. In Figures 2-14 to 2-20, assume one symbol duration $T=\frac{1}{2}$.

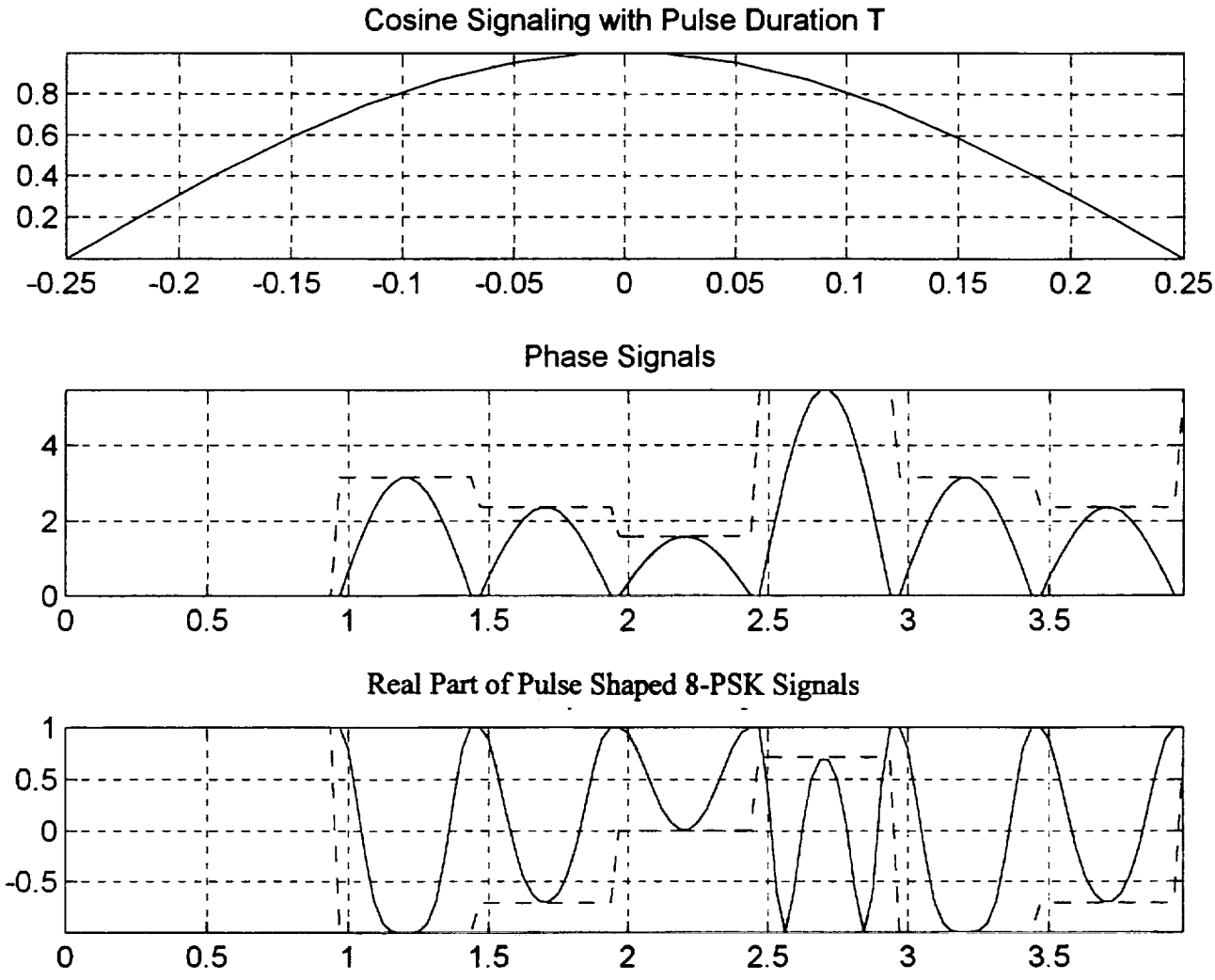

Figure 2-14 T Duration Cosine Pulse Used as Phase Pulse and 8-PSK Signaling

Cosine with Double-Interval Cosine with double interval can be expressed as

$$h(t)=\begin{cases} \cos(\pi \dfrac{t}{2T}) & |t| < T \\ 0 & |t| > T \end{cases} \qquad (2\text{-}41)$$

2T duration cosine pulse used as phase pulse and 8-PSK signaling are shown in Figure 2-15.

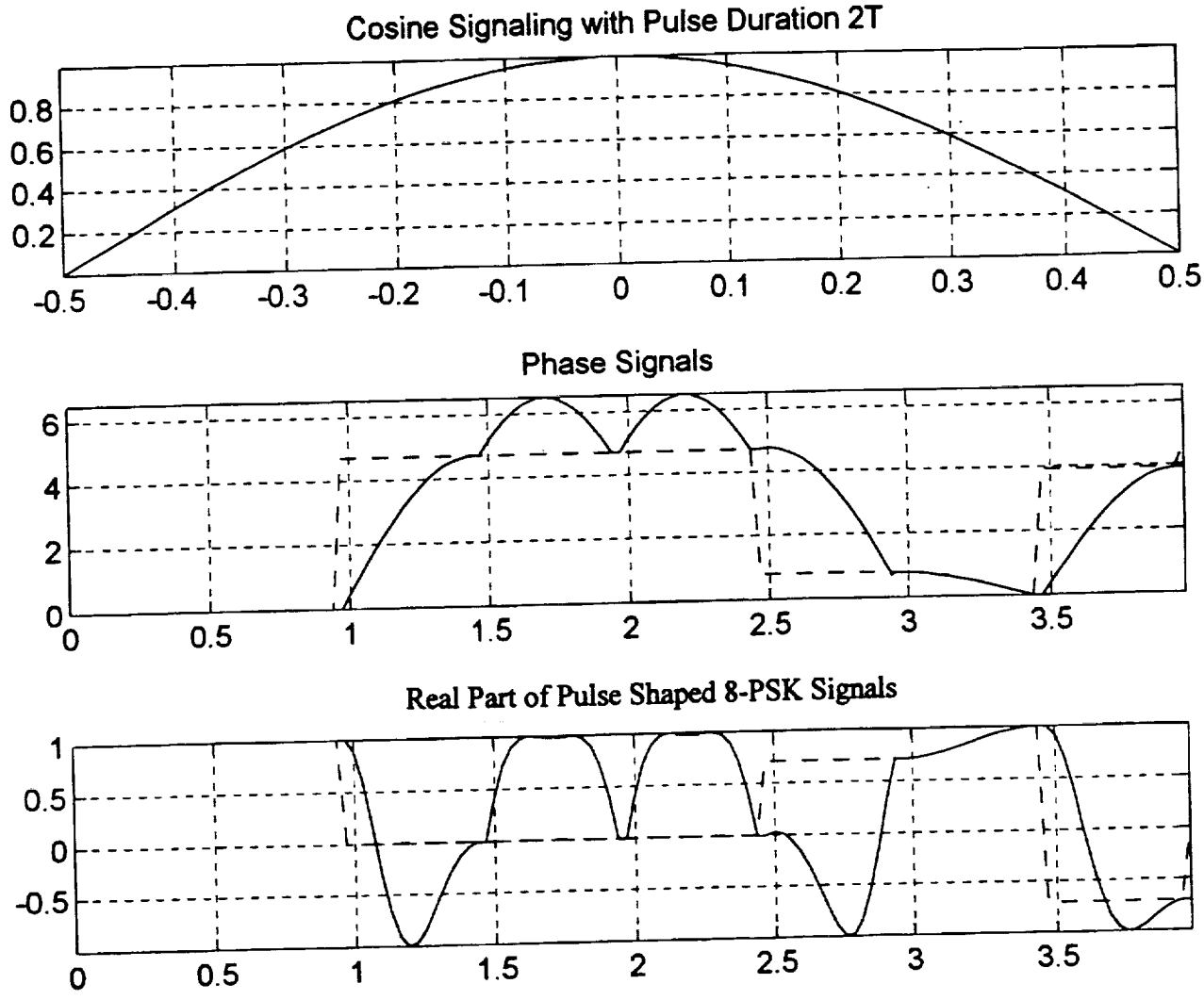

Figure 2-15 2T Duration Cosine Pulse Used as Phase Pulse and 8-PSK Signaling

Raised Cosine with Single-Interval Raised cosine with single interval can be expressed as

$$h(t)=\begin{cases}\cos^2(\pi t/T) & |t| \le \dfrac{T}{2} \\ 0 & |t| > \dfrac{T}{2}\end{cases} \qquad (2\text{-}42)$$

T duration raised cosine pulse used as phase pulse and 8-PSK signaling are shown in Figure 2-16

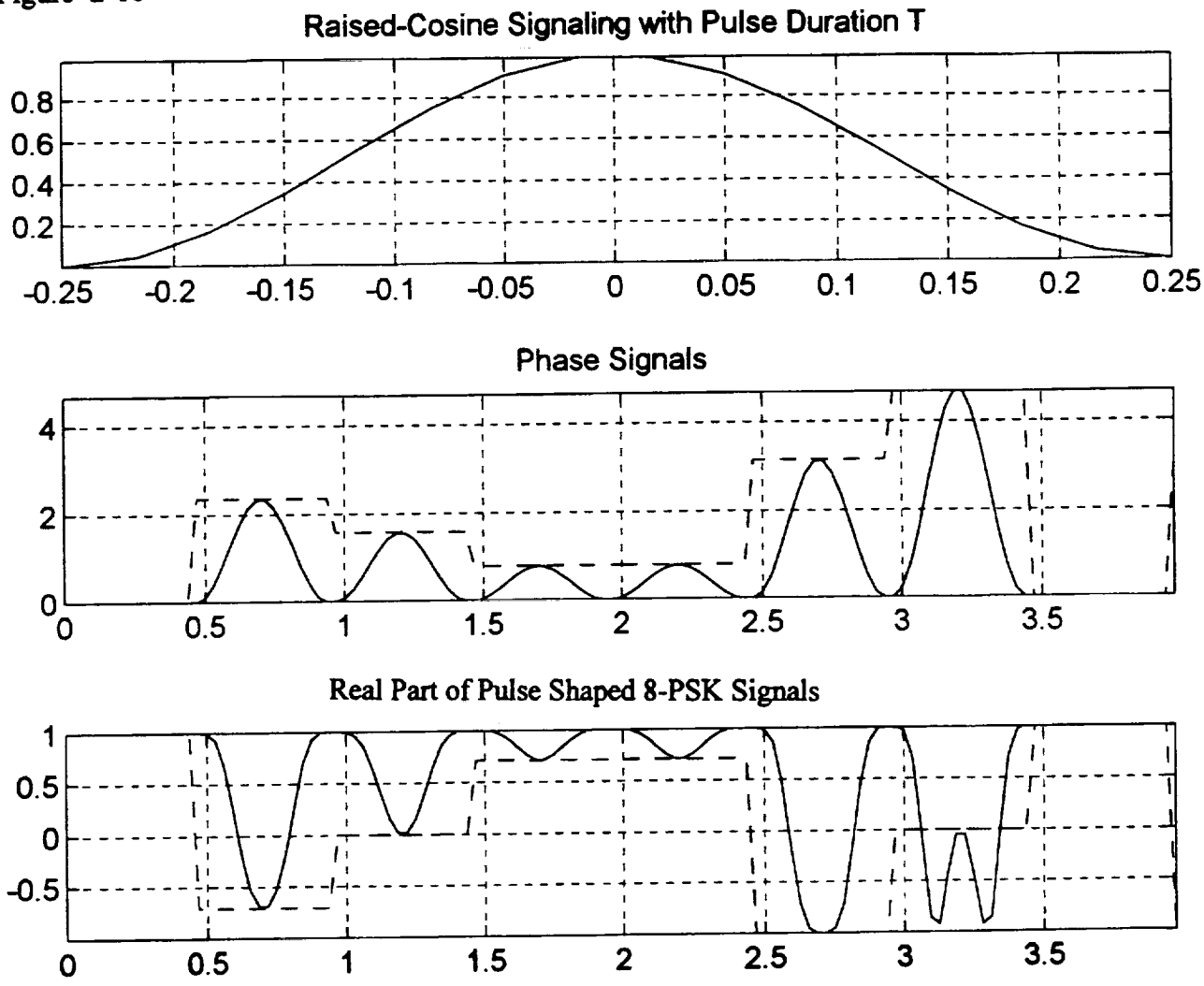

Figure 2-16 T Duration Raised Cosine Pulse Used as Phase Pulse and 8-PSK Signaling

Raised Cosine with Double-Interval Raised Cosine with double interval can be expressed as

$$h(t)=\begin{cases}\cos^2(\pi\dfrac{t}{2T}) & |t|\le T\\ 0 & |t|>T\end{cases} \qquad (2\text{-}43)$$

2T duration raised cosine pulse used as phase pulse and 8-PSK signaling in Figure 2-17.

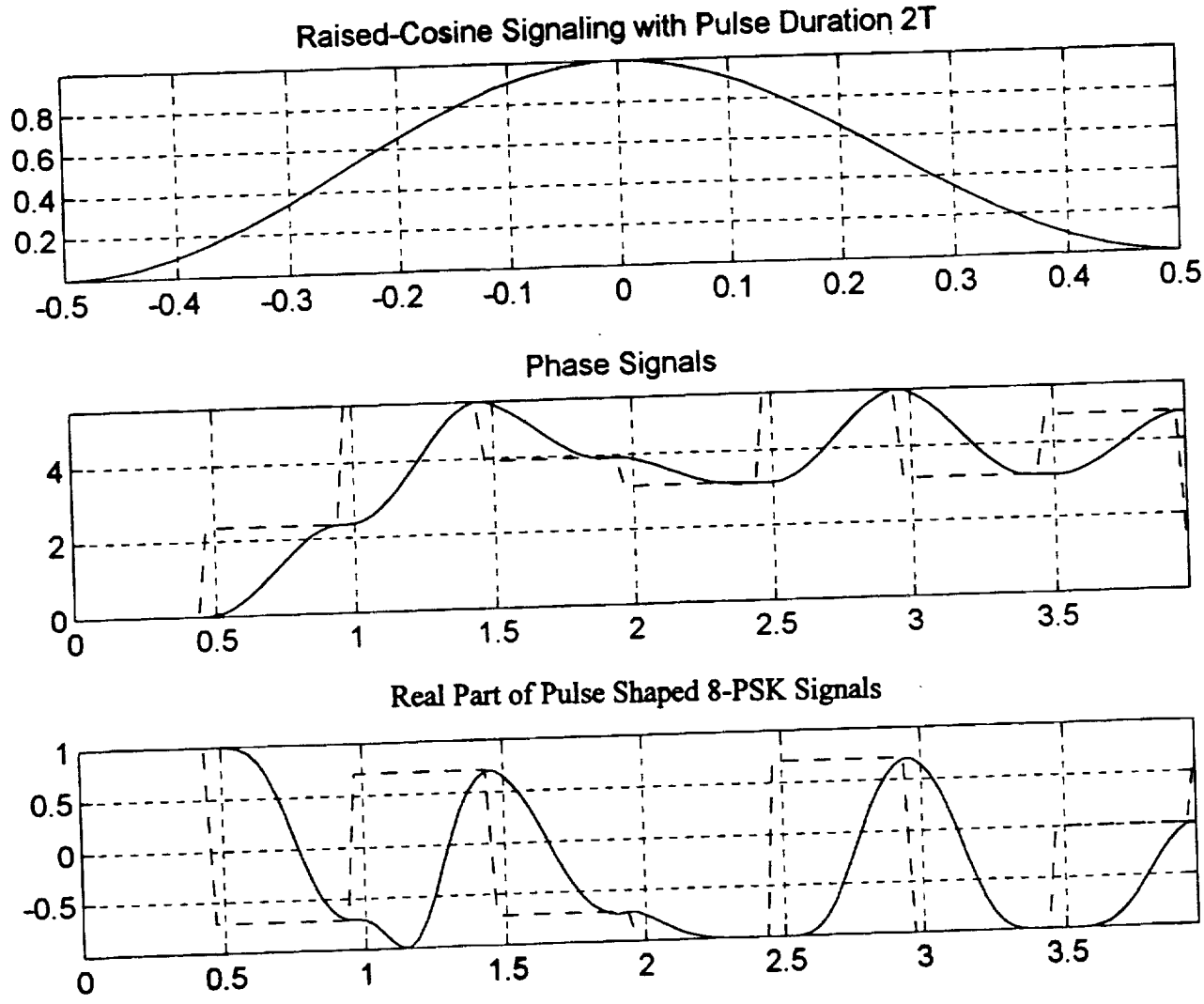

Figure 2-17 2T Duration Raised Cosine Pulse Used as Phase Pulse and 8-PSK Signaling

Weighted Raised Cosine with Double-Interval Weighted raised cosine [5] with double interval can be expressed as

$$h(t)=\begin{cases} \frac{1}{2}[\cos(\pi \frac{t}{T})] - \frac{1-k}{2}[1-\cos\frac{2\pi t}{T}] & |t| \le T \\ 0 & |t| > T \end{cases} \quad (2\text{-}44)$$

where $0.5 \le k \le 1.5$ $2T$ duration raised cosine pulse used as phase and 8-PSK signals are shown in Figure 2-18.

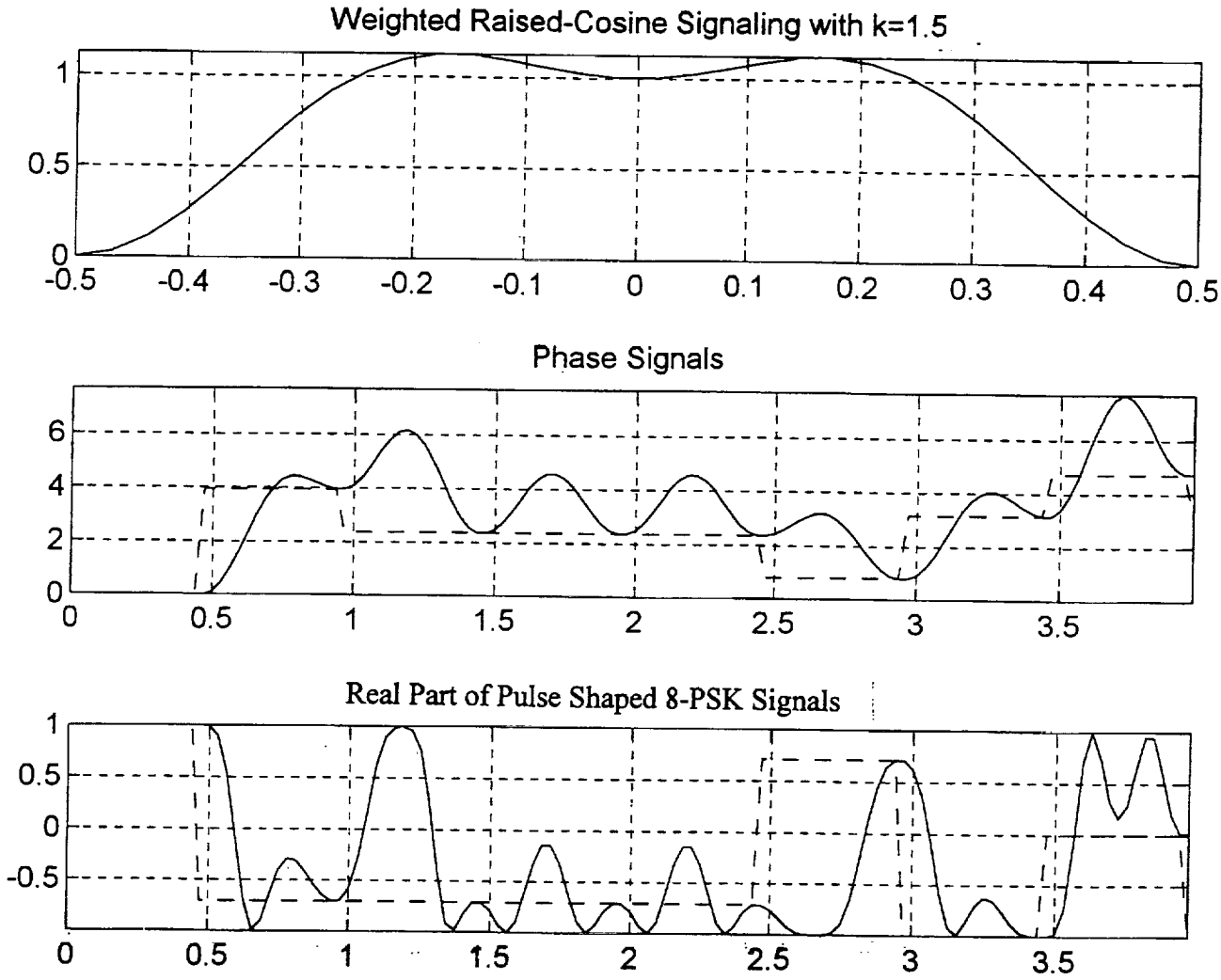

Figure 2-18 Weighted Raised Cosine Pulse Used as Phase Pulse and 8-PSK Signaling

Trapezoid Signaling A trapezoid signal can be expressed as

$$h(t)=\begin{cases} 1 & |t| < \frac{T}{2} \\ 2-\frac{2}{T}|t| & \frac{T}{2} \le |t| \le T \\ 0 & |t| > T \end{cases} \qquad (2\text{-}45)$$

where $0.5 \le k \le 1.5$

Trapezoid pulse used as phase and 8-PSK signals are shown in Figure 2-19.

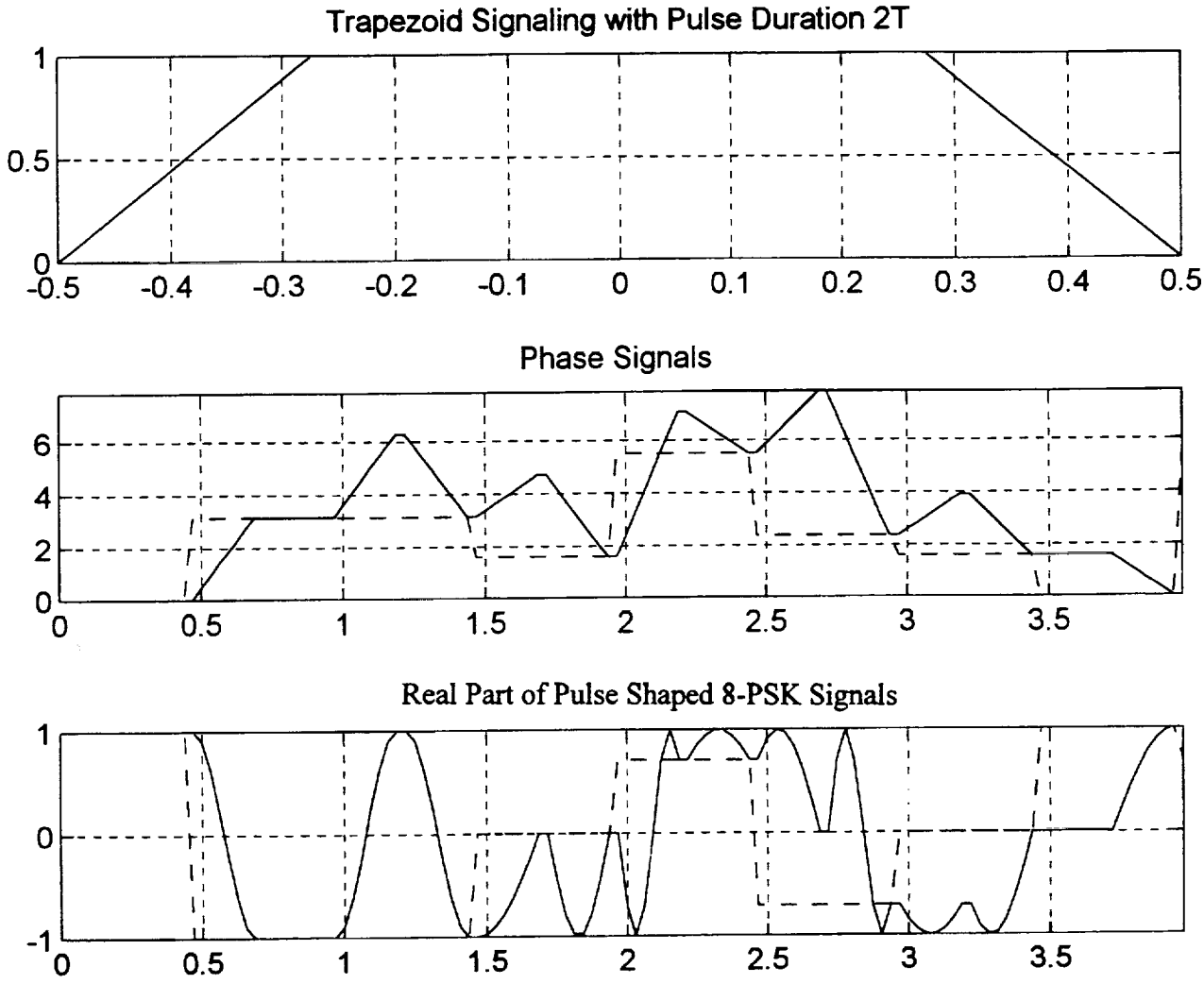

Figure 2-19 2T Duration Trapezoid Pulse Used as Phase Pulse and 8-PSK Signaling

Weighted Raised Cosine Transit Signaling A pulse with weighted raised cosine transit and flat within one symbol period can be expressed as

$$h(t)=\begin{cases} 1 & |t| < \frac{T}{2} \\ \frac{1}{2}[\cos(\pi \frac{t}{T})] - \frac{1-k}{2}[1-\cos\frac{2\pi t}{T}] & \frac{T}{2} \le |t| \le T \\ 0 & |t| > T \end{cases}$$

where $0.5 \le k \le 1.5$

The pulse with weighted raised cosine transit used as phase and 8-PSK signals are shown in Figure 2-20

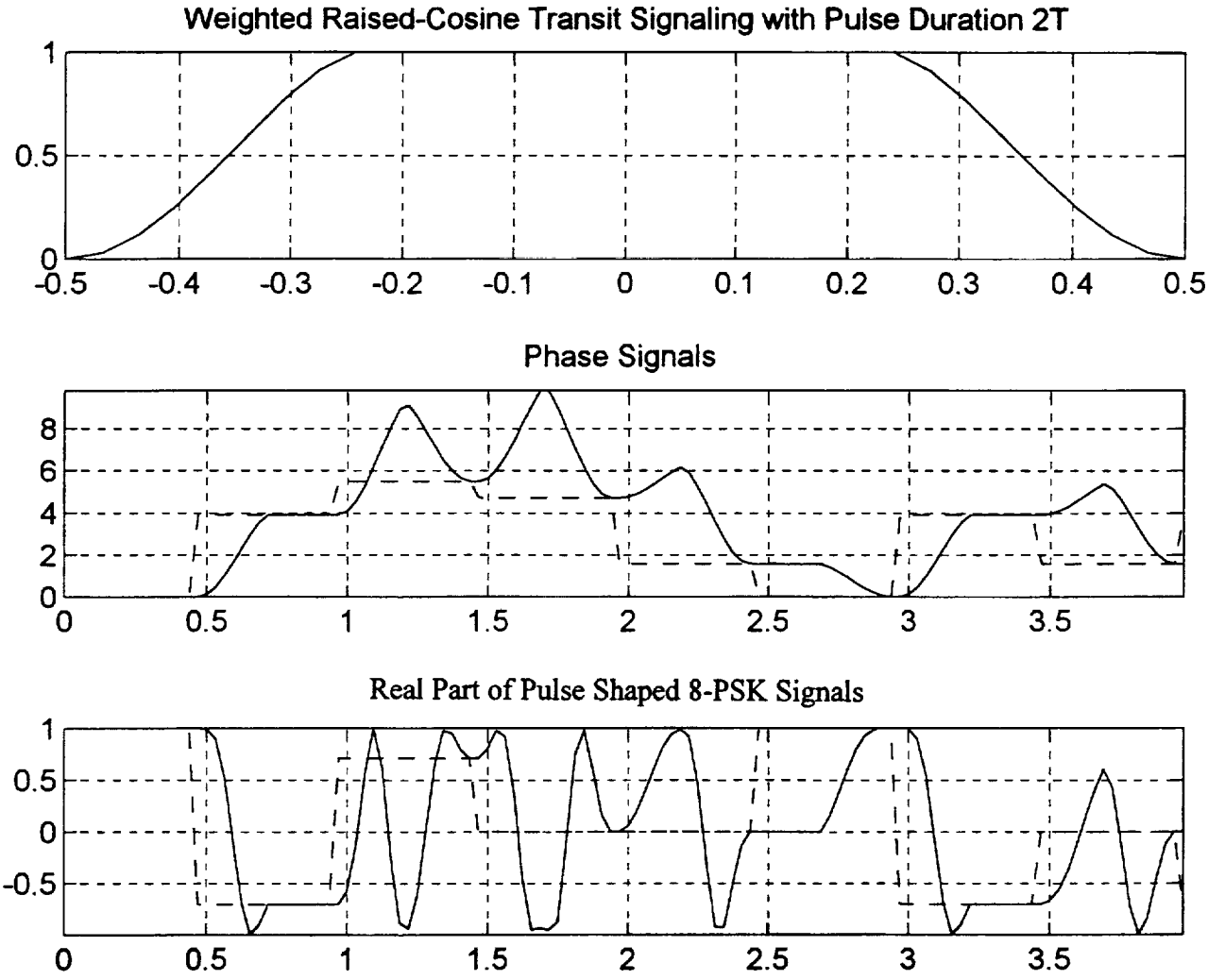

Figure 2-20 Weighted Raised Cosine Transit Pulse Used as Phase Pulse and 8-PSK Signaling

2.4 Solid State Power Amplifier (SSPA)

A Solid State Power Amplifier (SSPA) is used in the project. The magnitude and phase plots of the SSPA were obtained from JPL. From the plot (Figure 8), the SSPA has two main ranges which include a linear and non-linear region. If the input power is less than -5 dB, the SSPA is worked in the linear region, and the phase offset is approximately zero. If the input power is larger than -5 dB, the SSPA is working in the nonlinear region. This project sets the SSPA to work at saturation level of 0 dB.

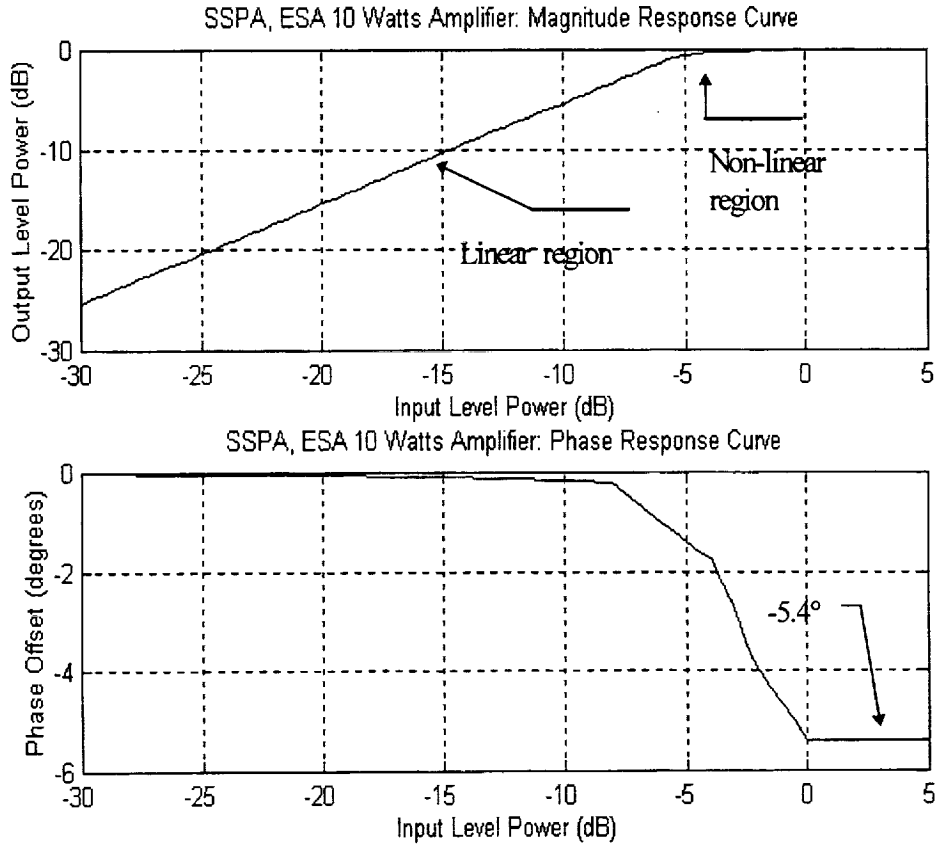

Figure 2-21 The Output Characteristic of 10 Watts SSPA

The main part of the SSPA simulation is an analytical Traveling Wave Tube (TWT) block which can simulate the nonlinear channel. By looking up the SSPA table file provided by JPL, the TWT realizes a conversion from input amplitude to output amplitude and input amplitude to output phase. Figure 2-22 shows the structure of the SSPA.

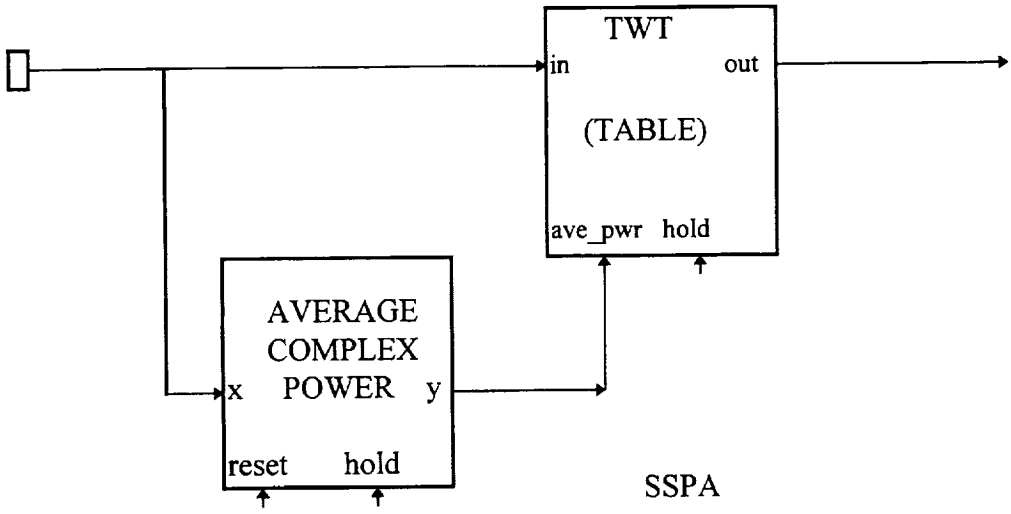

Figure 2-22 The Structure of SSPA.

2.5 Additive White Gaussian Noise Channel

Additive White Gaussian Noise (AWGN) is added to the signals out of the SSPA to

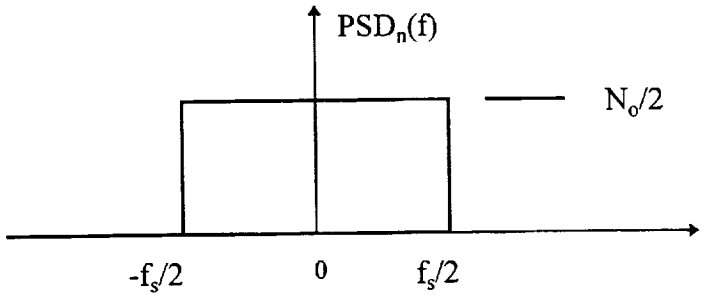

Figure 2-23 Power Spectral Density Of White Gaussian Noise.

simulate channel noise. Figure 2-23 Shows the power spectral density for the AWGN used in the simulation. Actual white noise has a flat spectrum from $-\infty$ to ∞. The AWGN is taken to have zero mean and with variance $\sigma_n^2 = N_0/2$. $N_0/2$ is the power spectral density of the white noise, and F_s is the sampling frequency.

2.6 Receiver and Error Rate Estimation System

There are three parts in the receiver and estimation system, receiver, synchronizer and error rate estimator. Figure 2-24 shows the block diagram for this system.

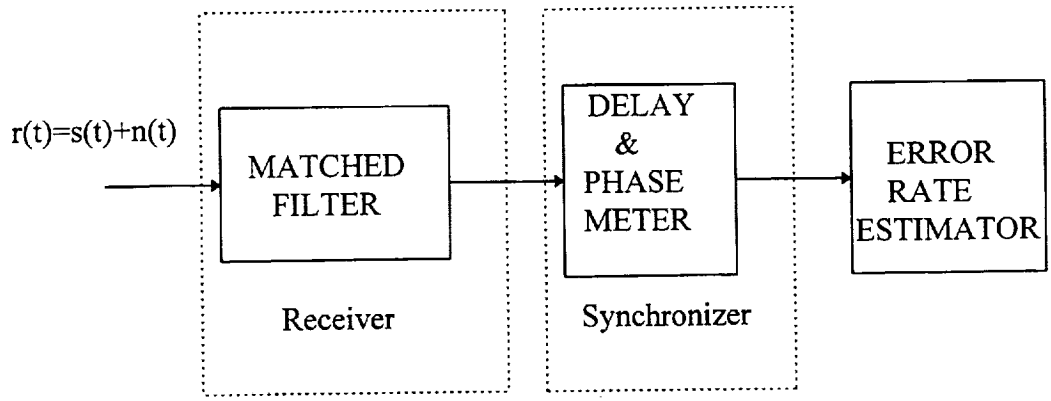

Figure 2-24 Block Diagram for the Receiver Error Rate Estimator

Receiver In an ideal receiver, a matched filter is used. The matched filter is a linear filter which maximizes the signal to noise ratio (SNR). In this project, an integrate and dump block (which match only a rectangular pulse) is used as the receiver.

Synchronizer The synchronizer performs a correlation between the reference signals and received signals (delayed and distorted), and gives an estimate of the number of samples of delay and the phase between the two samples. The reference signal is then delayed the same number of samples so that the two signals can be compared to get the error rate. Figure 2-25 shows the block diagram for the synchronization. The DELAY & PHASE METER can detect the number of sample delays of the received signals. The COMPLEX VARIABLE DELAY lets the reference signals be delayed by the same number of samples as the received signal so they can be compared in the error rate estimator.

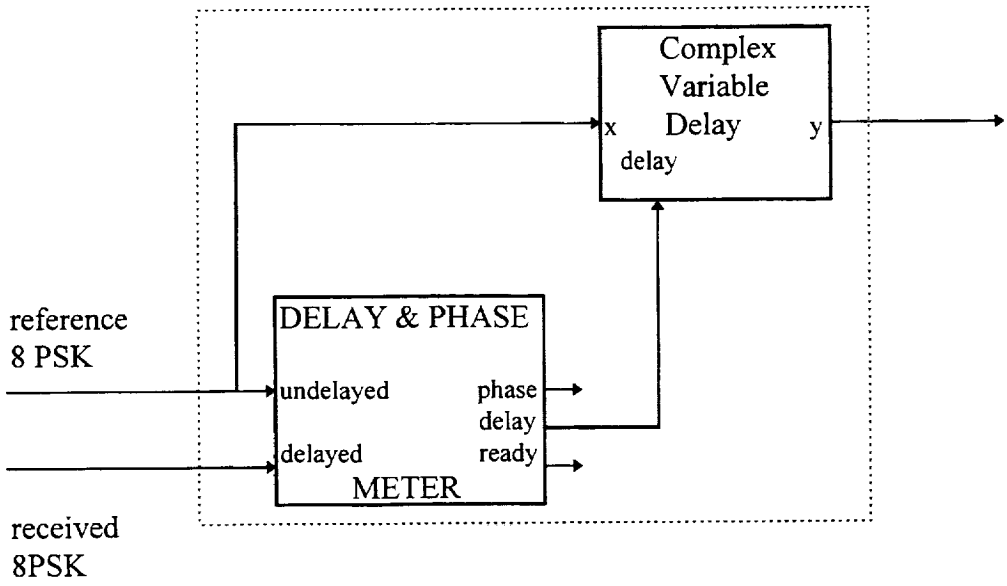

Figure 2-25 Block Diagram of Synchronizer

Error Rate Estimator The reference signal and received signal (now having the same delay), are put into the error rate estimator to count the number of bit errors. The

main block used to count bit errors is SIMPLE ERROR RATE ESTIMATOR(Figure 2-26) which compares the reference and the received signals to find bit errors.

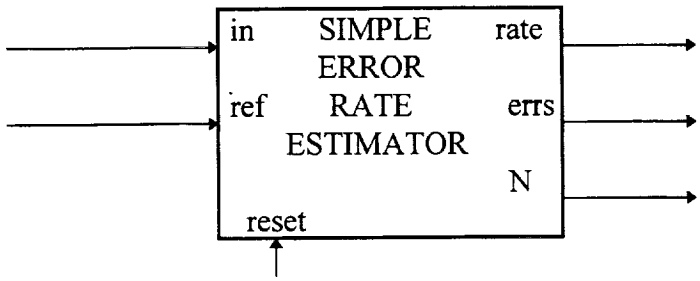

Figure 2-26 Simple Error Rate Estimator Block Diagram

Chapter 3

PULSE SHAPED 8-PSK SIMULATIONS

This chapter will provide simulation procedures and results of pre-pulse shaped 8-PSK. Simulations included power spectral density (PSD) and bit error rates (BER). In addition to simulating traditional filters, some particular 8-PSK waveforms will first be simulated to eliminate power spectral spikes.

3.1 Simulations on Power Spectral Density

Figure 3-1 shows the procedure for obtaining the power spectra for pre-pulse shaped 8-PSK signal.

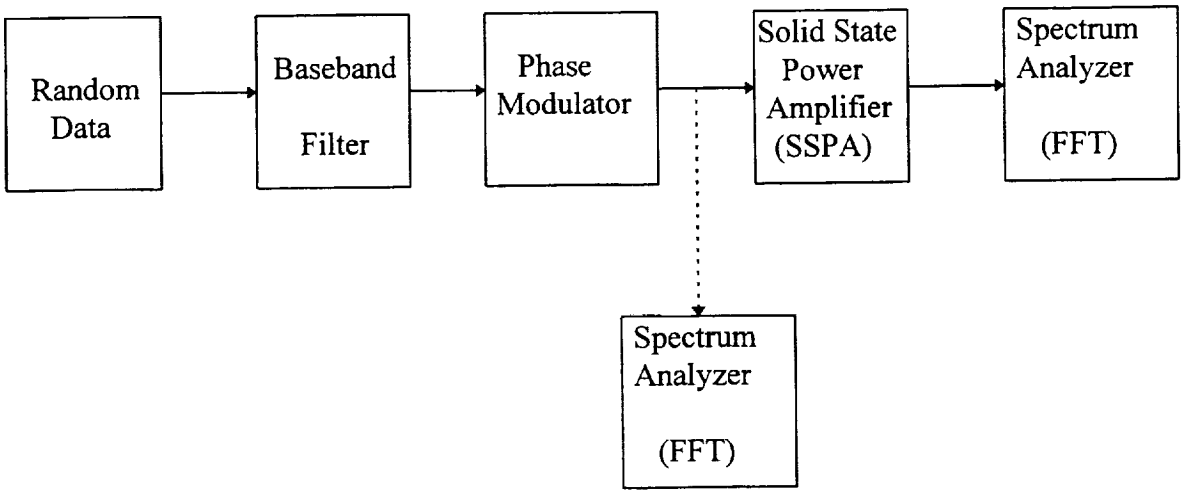

Figure 3-1 Block Diagram of Spectrum Analysis

The random data source provides ideal data with a symbol rate (R_s), and the sample frequency, Fs, is $512R_s$ Hz. For the pulse shaping, traditional filters and particular

filters are used. For Butterworth and Bessel filters, bandwidth (BT) is equal to the cutoff frequency which corresponds to the -3dB amplitude point. The BT represents the product of the bandwidth with the symbol time. Traditional filters used in the simulations are in Table 3-1.

Table 3-1 Traditional Filters Used in the Simulation

Filters	BTs or roll-off factor (α)			
5th-Order Butterworth	BT=1	BT=2	BT=2.8	BT=3
3rd-Order Bessel	BT=1	BT=1.2	BT=2	BT=3
SRRC	α=1			

Particular 8-PSK waveforms, such as trapezoid, weighted raised cosine transit signaling, cosine transit and raised cosine transit signaling, are also investigated to test their ability to get rid of or reduce spectral spikes. The constant envelope pulse shaped 8-PSK signal which comes from modulator goes to the input of the Solid State Power Amplifier (SSPA).

The spectrum Analyzer can be put before and after the SSPA. Since the SSPA is worked at the saturation level and a constant envelope 8-PSK signal is used, the spectrum of the signals at the input of the SSPA is almost the same as that of the signal output from the SSPA. The power spectrum is obtained by taking the Fourier Transform of the input signals of length 131072, using a Bartlett window. The power spectrum is then estimated by averaging 100 such FFTs.

3.1.1 PSD Simulation Results of Using Traditional Filters

The plots of the power spectra are given in Figures 3-2 to Figure 3-11. The following parameters were used to obtain the power spectra.

Data Source :

a. Ideal data with p(0) (probability of zero)=0.5;

c. Sample Rate (f_s) =512R_s Hz

Traditional Filters for Pulse Shaping:

a. None

b. Butterworth 5th Order (BT=1,2,2.8,3)

c. Bessel 3rd Order (BT=1,1.2,2,3)

d. SRRC (α =1, Number of tap length=32*R_s=8192, Bartlett window

Power Amplifier:

European Space Agency (ESA) 10-watt SSPA

SPW Spectrum Analyzer

a. FFT length=512R_s

b. Window type: Bartlett

c. Average: 100 FFTs

d. Sampling frequency =512R_s Hz

Spectrum Plots Ranges

$\pm 10\ R_b$; $\pm 75\ R_b$

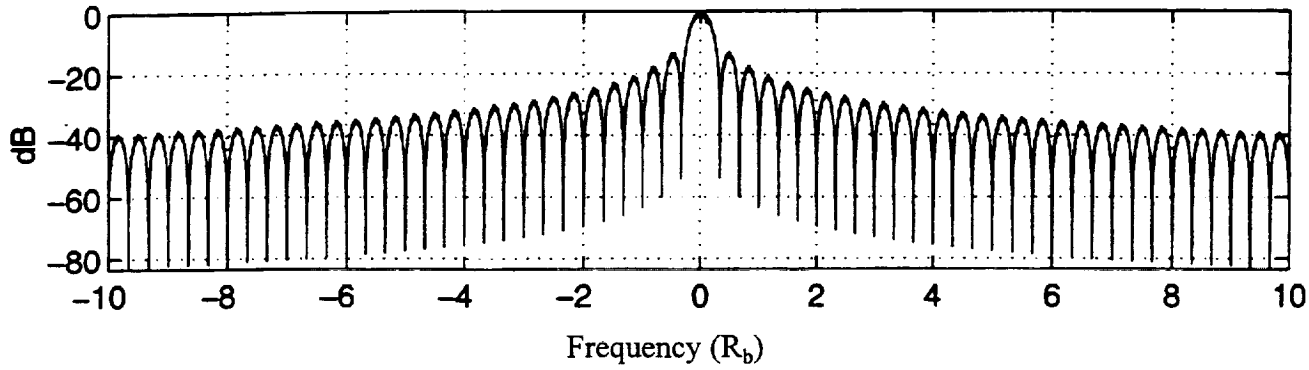

(a) Unfiltered 8 PSK $\pm 10\ R_b$

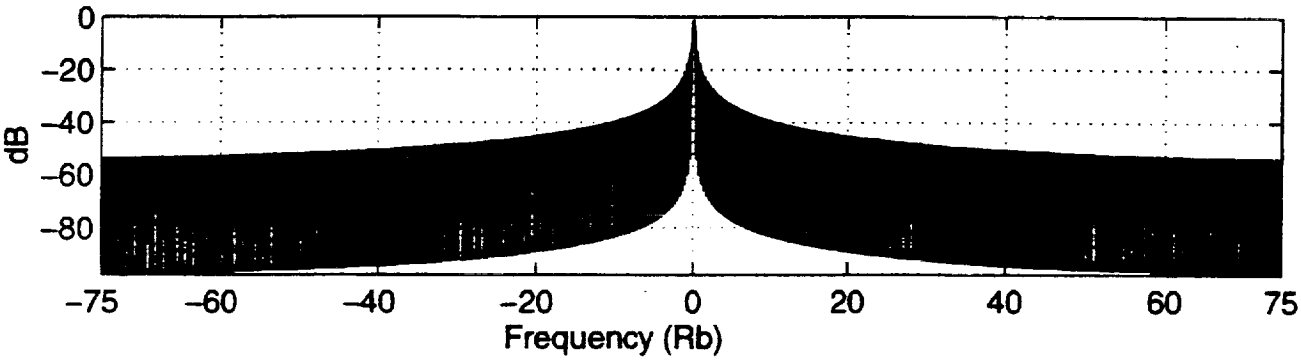

(b) Unfiltered 8 PSK $\pm 75\ R_b$

Figure 3-2 Unfiltered 8-PSK Power Spectral Density

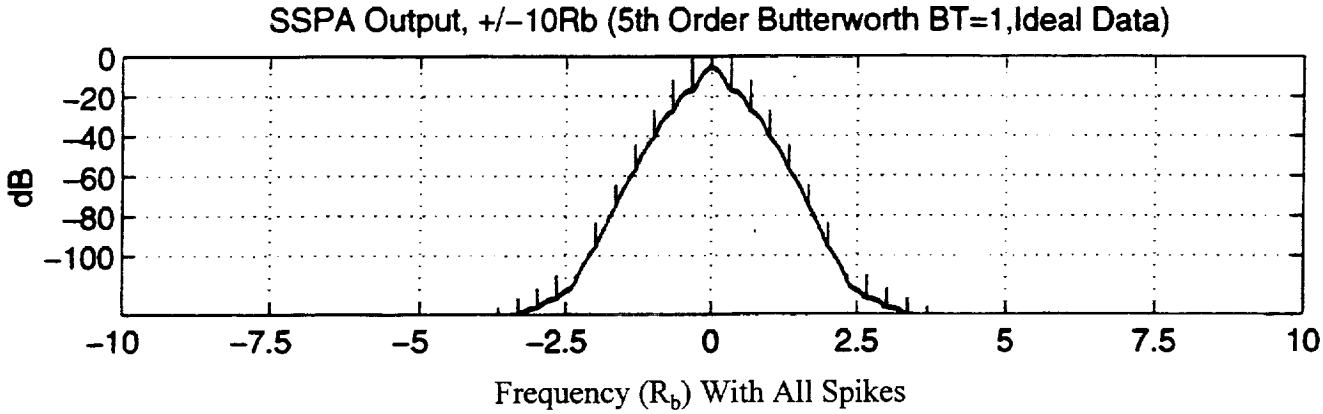

(a) 5th Order Butterworth Filter (BT=1), $\pm 10\ R_b$

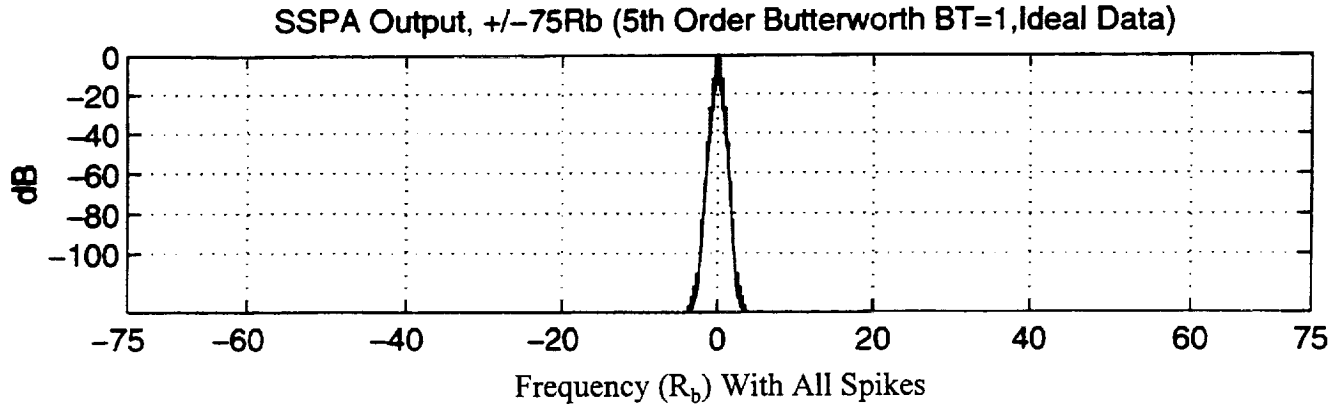

(b) 5th Order Butterworth Filter (BT=1) , $\pm 75R_b$

Figure 3-3 Power Spectra of 8-PSK Pulse Shaped with 5th-order Butterworth filter (BT=1)

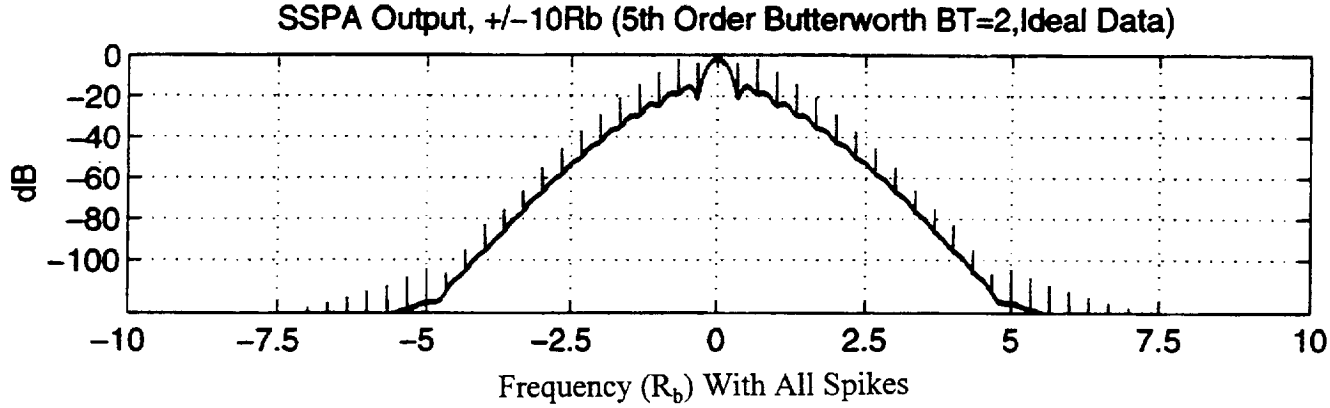

(a) 5th Order Butterworth Filter (BT=2) , $\pm 10R_b$

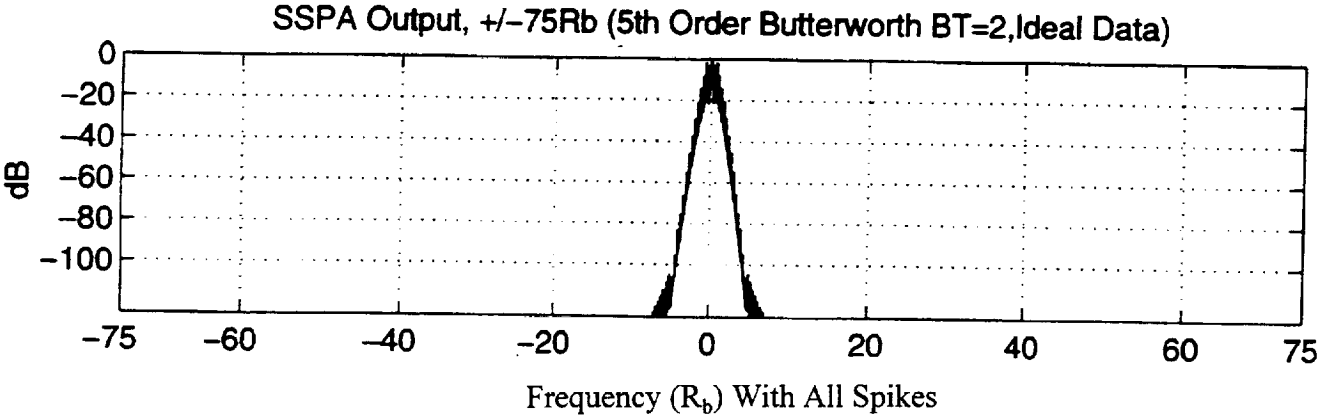

(b) 5th Order Butterworth Filter (BT=2) , $\pm 75R_b$

Figure 3-4 Power Spectra of 8-PSK Pulse Shaped with 5th-order Butterworth filter (BT=2)

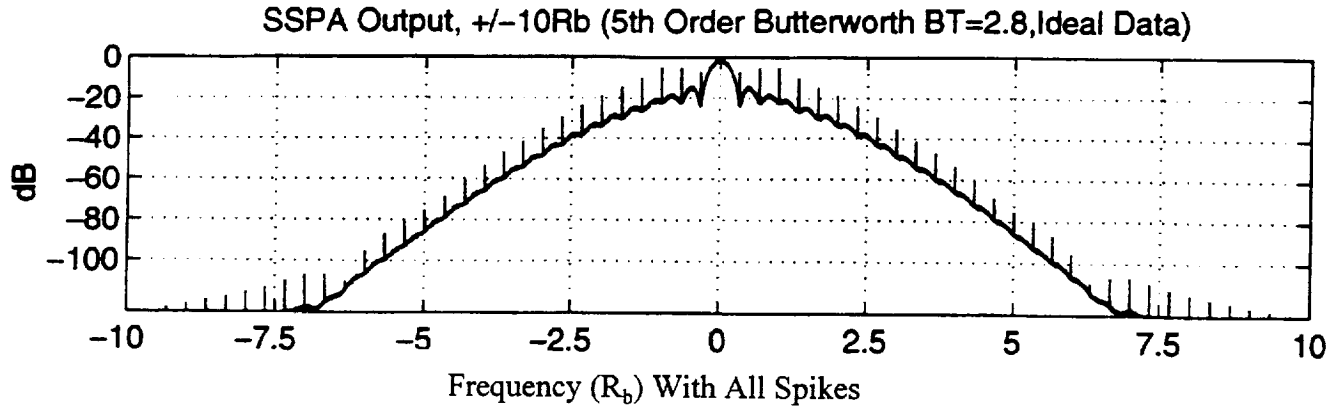

(a) 5th Order Butterworth Filter (BT=2.8), $\pm 10R_b$

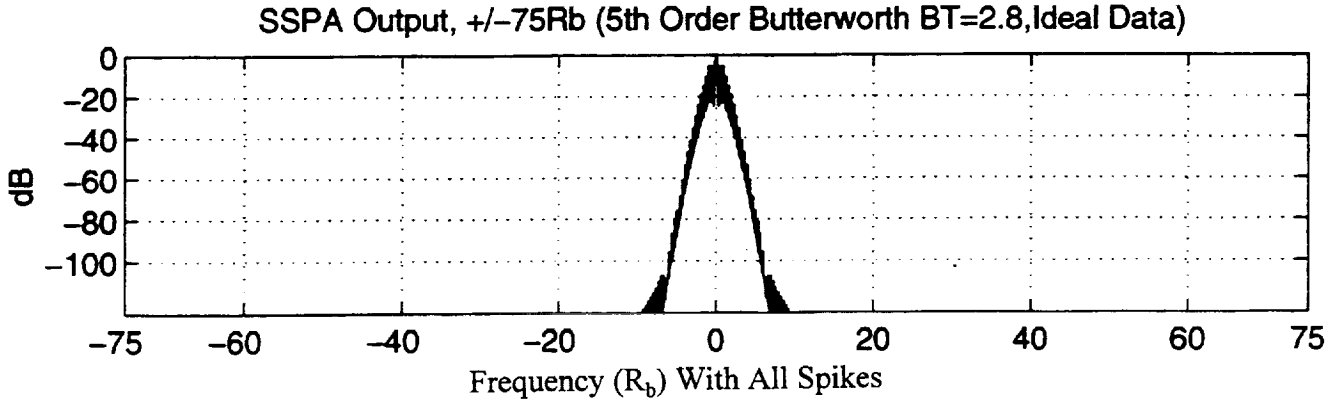

(b)5th Order Butterworth Filter (BT=2.8), $\pm 75R_b$

Figure 3-5 Power Spectra of 8-PSK Pulse Shaped with 5th-order Butterworth filter (BT=2.8)

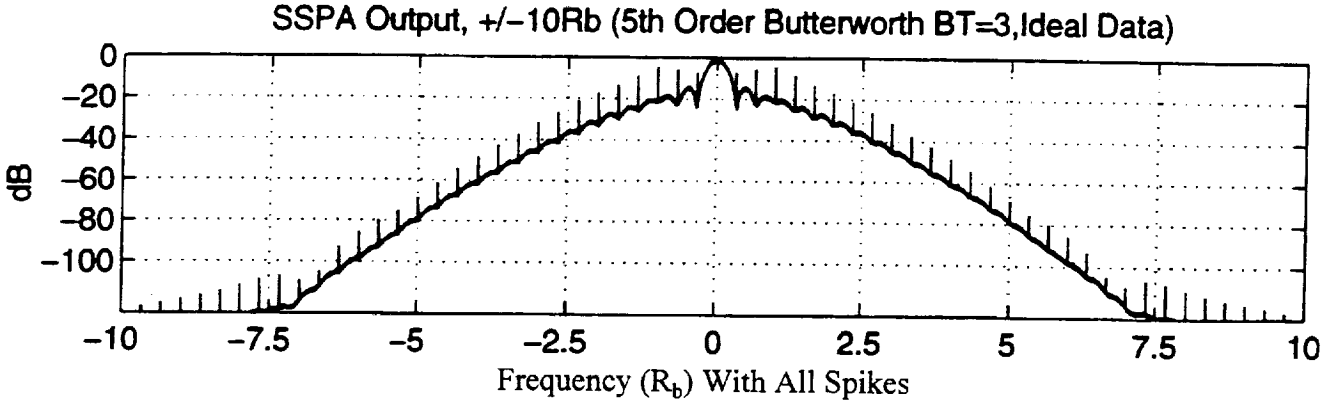

(a) 5th Order Butterworth Filter (BT=3), $\pm 10R_b$

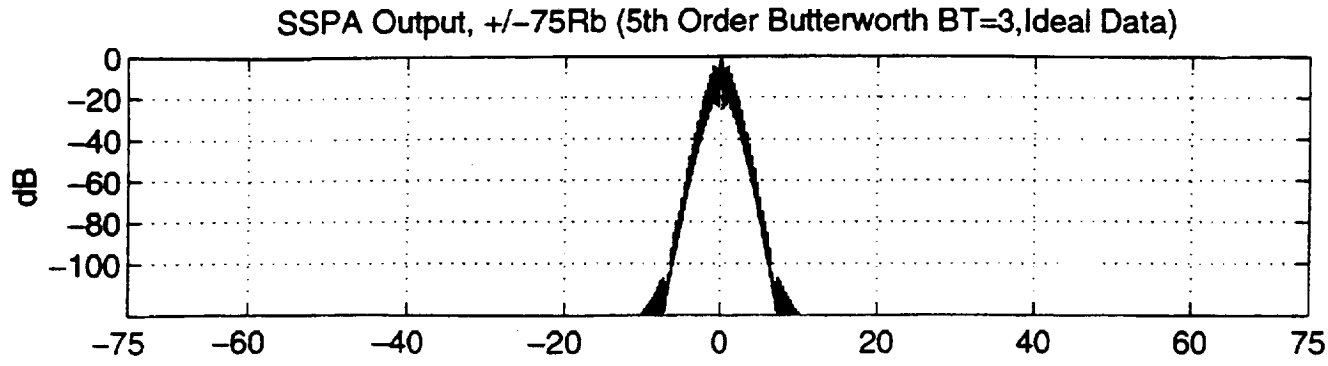

(b) 5th Order Butterworth Filter (BT=3), ± 75R_b

Figure 3-6 Power Spectra of 8-PSK Pulse Shaped with 5th-order Butterworth filter (BT=3)

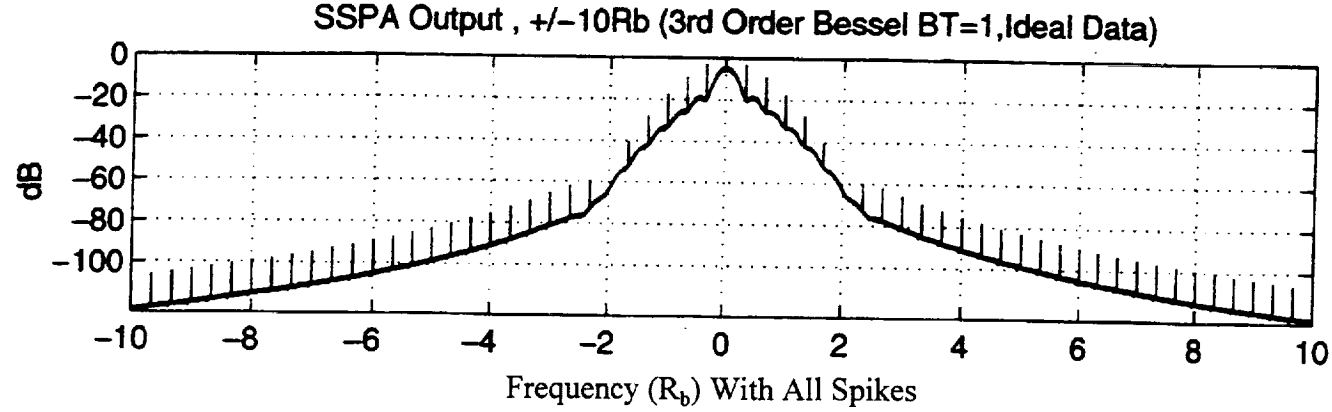

(a) 3rd Order Bessel Filter (BT=1) , ± 10R_b

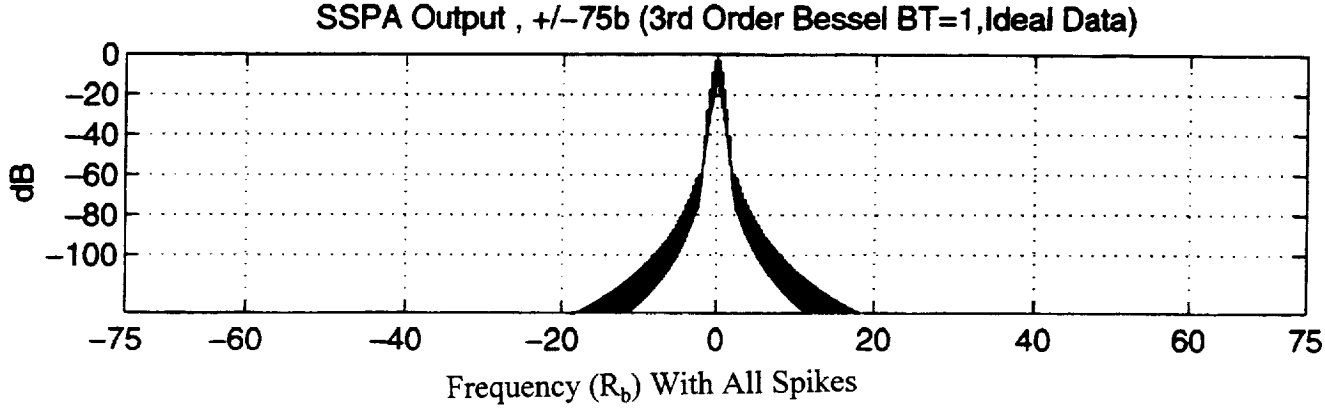

(b) 3rd Order Bessel Filter (BT=1), ± 75R_b

Figure 3-7 Power Spectra of 8-PSK Pulse Shaped with 3rd-order Bessel filter (BT=1)

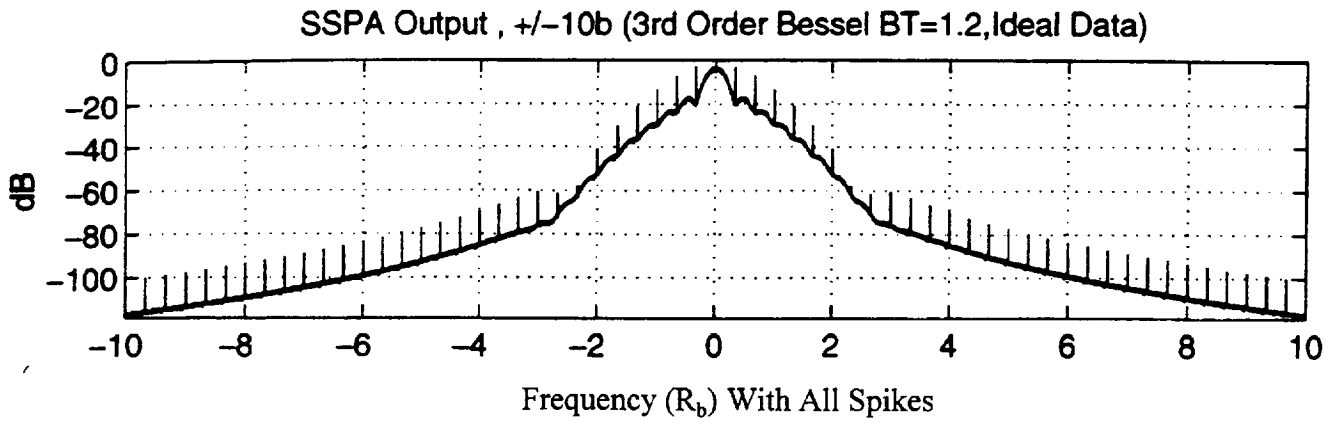

(a) 3rd Order Bessel Filter (BT=1.2), $\pm 10R_b$

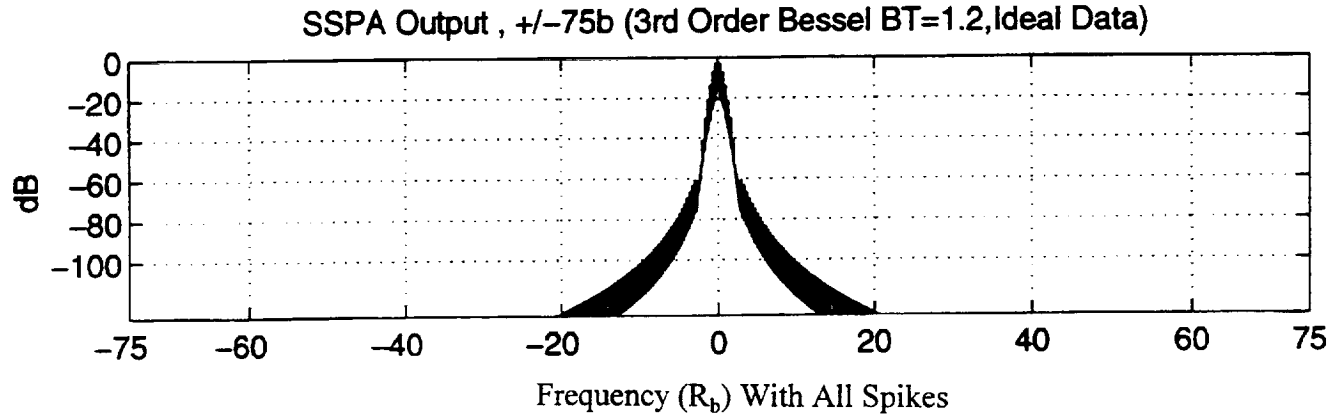

(b) 3rd Order Bessel Filter (BT=1.2) , $\pm 75R_b$

Figure 3-8 Power Spectra of 8-PSK Pulse Shaped with 3rd-order Bessel filter (BT=1.2)

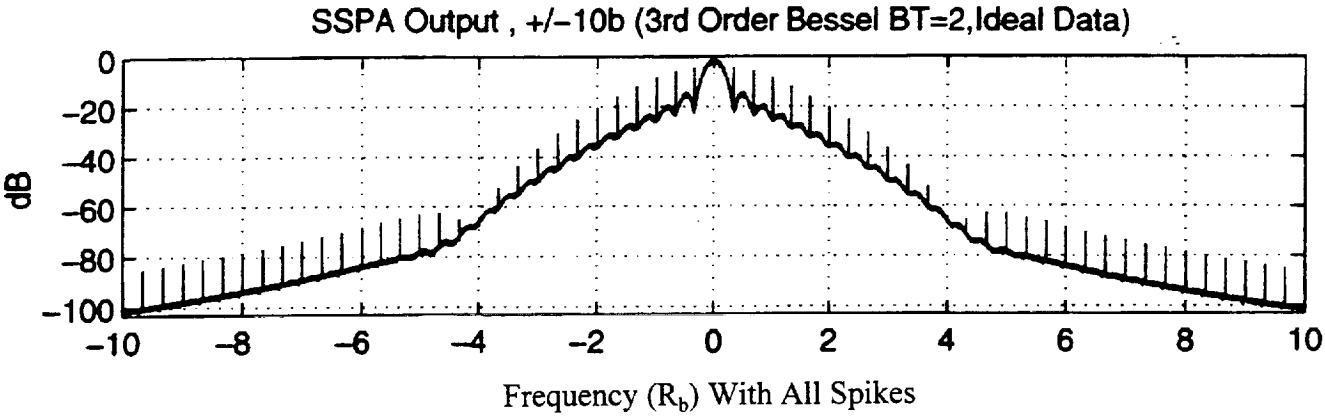

(a) 3rd Order Bessel Filter (BT=2), $\pm 10R_b$

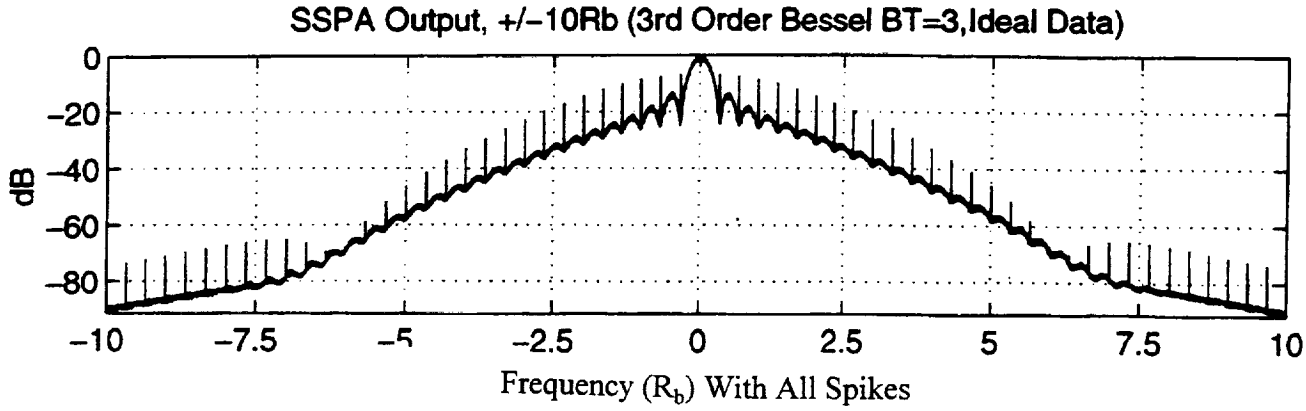

(a) 3rd Order Bessel Filter (BT=3), ± 10R_b

Figure 3-9 Power Spectra of 8-PSK Pulse Shaped with 3rd-order Bessel filter (BT=2)

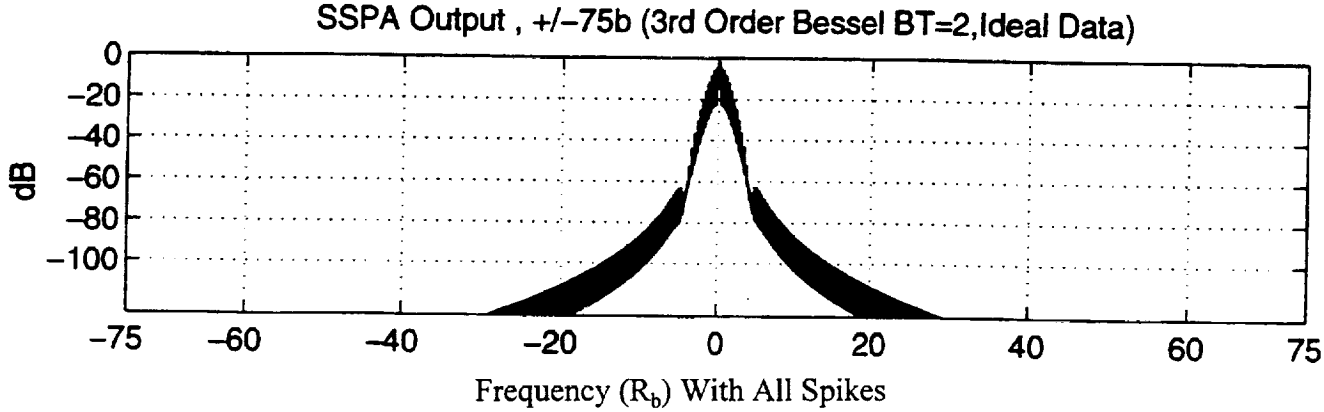

(b) 3rd Order Bessel Filter (BT=2) , ± 75R_b

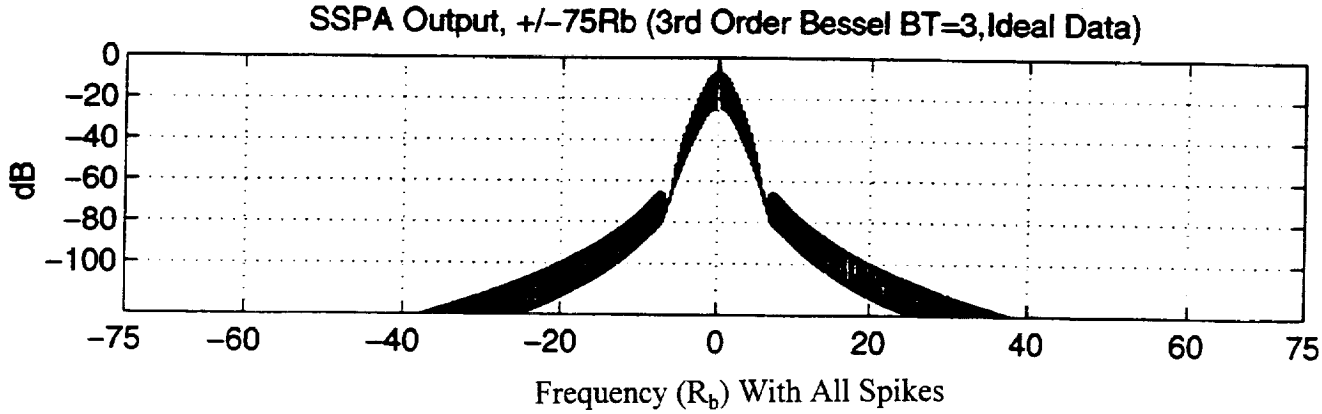

(b) 3rd Order Bessel Filter (BT=3), ± 75R_b

Figure 3-10 Power Spectra of 8-PSK Pulse Shaped with 3rd-order Bessel filter (BT=3)

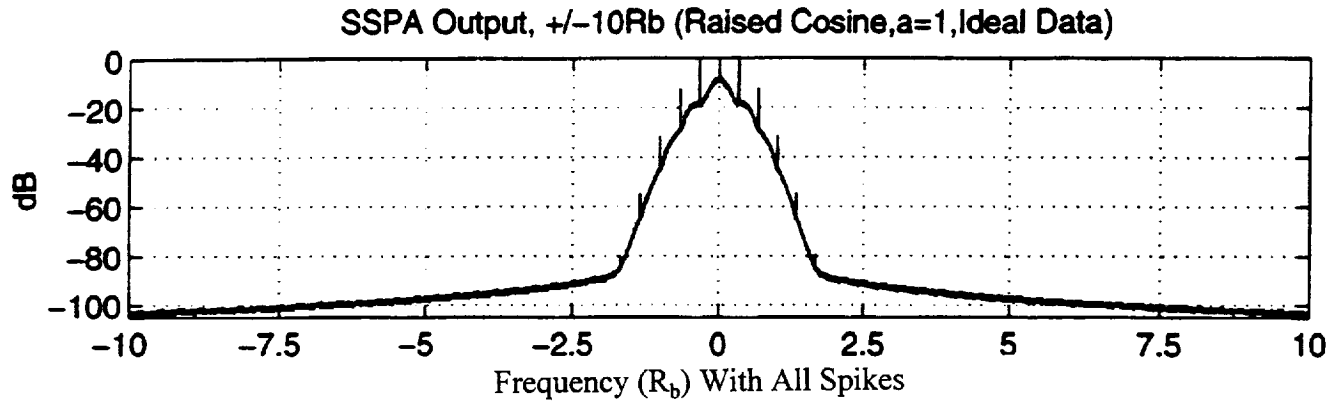

(a) Square-Root Raised Cosine (α =1) , $\pm 10R_b$

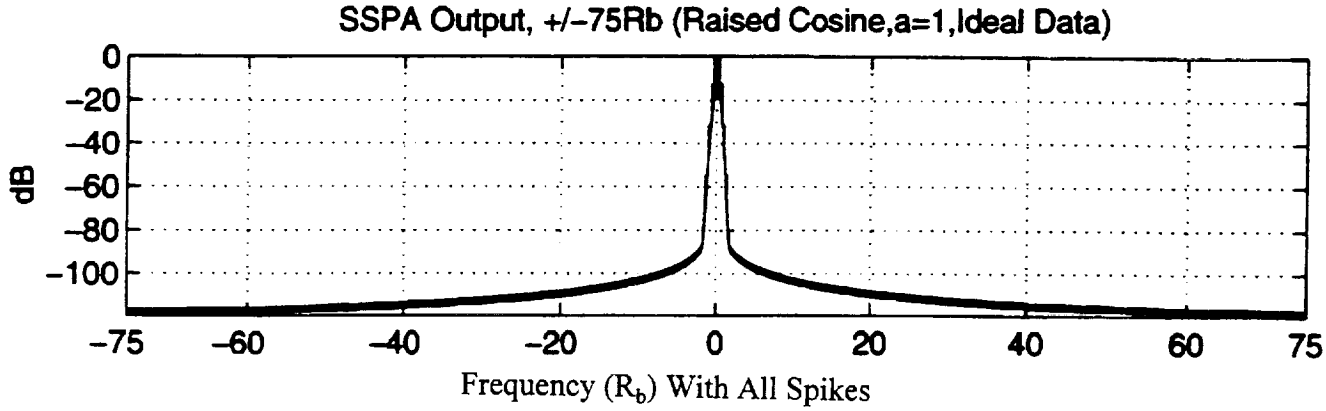

(b) Square-Root Raised Cosine (α =1) , $\pm 75R_b$

Figure 3-11 Power Spectra of 8-PSK Pulse Shaped with SRRC filter (α =1)

3.1.2 PSD Comparison Between Two Pulse Shaping Methods

The PSD related to pre-modulation pulse shaping will be compared with simulations using post-modulation pulse shaping. In order to compare the effect of two methods, a frequency band utilization ratio ρ [16] can be defined as:

$$\rho = \frac{\text{Number of spacecraft with Filtering Accommodated in Frequency Band}}{\text{Number of spacecraft without Filtering Accommodated in Frequency Band}}$$

An important assumption in deriving this ratio was made: the "spectra from spacecraft in adjacent channels will be permitted to overlap one another provided that, at the frequency where the overlap occurs, the signals are at least 50 dB below that of the main telemetry lobe (1st data sideband)." [16].

The Power Spectrum plots were used to determine this 50 dB level. For example, for 8-PSK signals without a pulse shaping , the -50dB point is situated at approximately 35 R_b and using the Butterworth Filter (BT=1), the -50 dB point is approximately at 1.28 R_b, then the Utilization ratio, ρ, is equal to

$$\rho = \frac{35R_b}{1.28R_b} = 27.34$$

From the simulations, the utilization ratios of pre-modulation pulse shaping were calculated and listed in Table 3-3 along with the utilization ratios for post-modulation pulse shaping [6]. From the utilization ratio table and Figure 3-12 to 3-13, for the same BT and baseband filters, pre-modulation pulse shaping has a higher band utilization ratio than that of post-modulation pulse shaping. Although the pre-modulation pulse shaping method has a narrower bandwidth, it produces spikes which are discrete line components of power

spectral density at particular frequencies. Figure 3-14 gives a PSD comparison of two methods with 5th-order butterworth filter.

Table 3-2 Utilization Ratio for Post-Modulation Pulse Shaping 8-PSK

Filter Type	-50 dB point (R_b)	Utilization
None	35	1
Butterworth(5th order)BT=1	2.5	14
Besssel (3rd order) BT=1	2.95	11.86
SRRC rolloff=1	2.5	14

Table 3-3 Utilization Ratio of Pre-Modulation Pulse Shaping 8-PSK

Filter Type	-50 dB point (R_b)	Utilization
None	35	1
Butterworth(5th order) BT=1	1.28	27
Butterworth(5th order) BT=2	2.43	14.4
Butterworth (5th order) BT=2.8	3.23	10.8
Butterworth (5th order) BT=3	3.45	10.1
Besssel (3rd order) BT=1	1.75	20
Besssel (3rd order) BT=1.2	2.04	17.1
Besssel (3rd order) BT=2	3.22	10.8
Besssel (3rd order) BT=3	4.53	7.7
SRRC rolloff=1	1.23	28.5

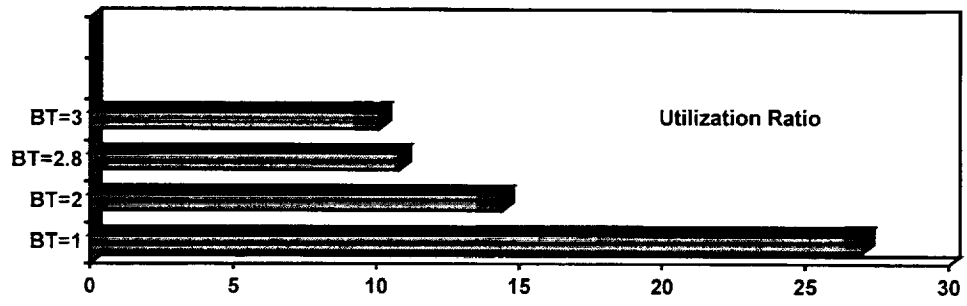

Figure 3-12 Utilization Ratio of Using 5th-Order Butterworth filters in Pre-Modulation Pulse Shaping

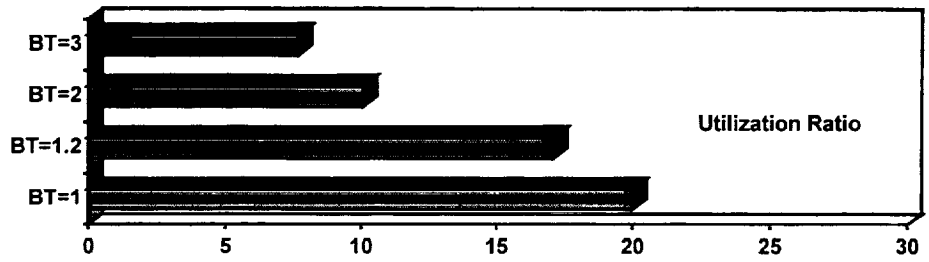

Figure 3-13 Utilization Ratio of Using 3rd-Order Bessel filters in Pre-Modulation Pulse Shaping

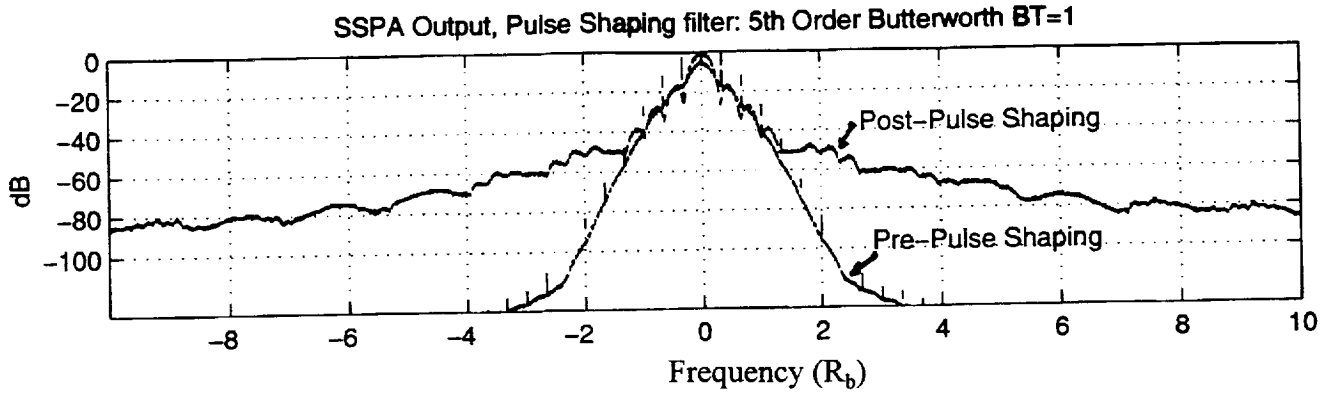

Figure 3-14 PSD Comparison of 8-PSK Between Two Pulse Shaping Methods (5th Order Butterworth Filter ,BT=1)

3.1.3 Simulation Results of Particular 8-PSK Waveforms

In order to reduce power spectral spikes produced by the pre-modulation pulse shaping method, some particular filters (8-PSK waveforms) were simulated. Since Greenstein [4] has already shown that triangular, cosine, raised cosine and Nyquist waveforms could not eliminate spectral spikes, formula (2-37) indicated that new

waveforms have to be investigated to get rid of spikes. The simulation parameters are the same as in section 3.1.1 except for different filters (waveforms) as follows.

8-PSK Particular Pulse Shaping Signaling

a. Trapezoid Signaling (2T and 3T duration)

b. Cosine Transit Signaling (2T duration)

c. Raised Cosine Transit Signaling (2T duration)

d. Weighted Raised Cosine Transit Signaling (2T duration)

The above waveforms share a common characteristic, that is to keep flat within one symbol time T. Figures 3-15 to Figure 3-19 show these particular waveforms not only can reduce bandwidth but also can eliminate or reduce spectral spikes.

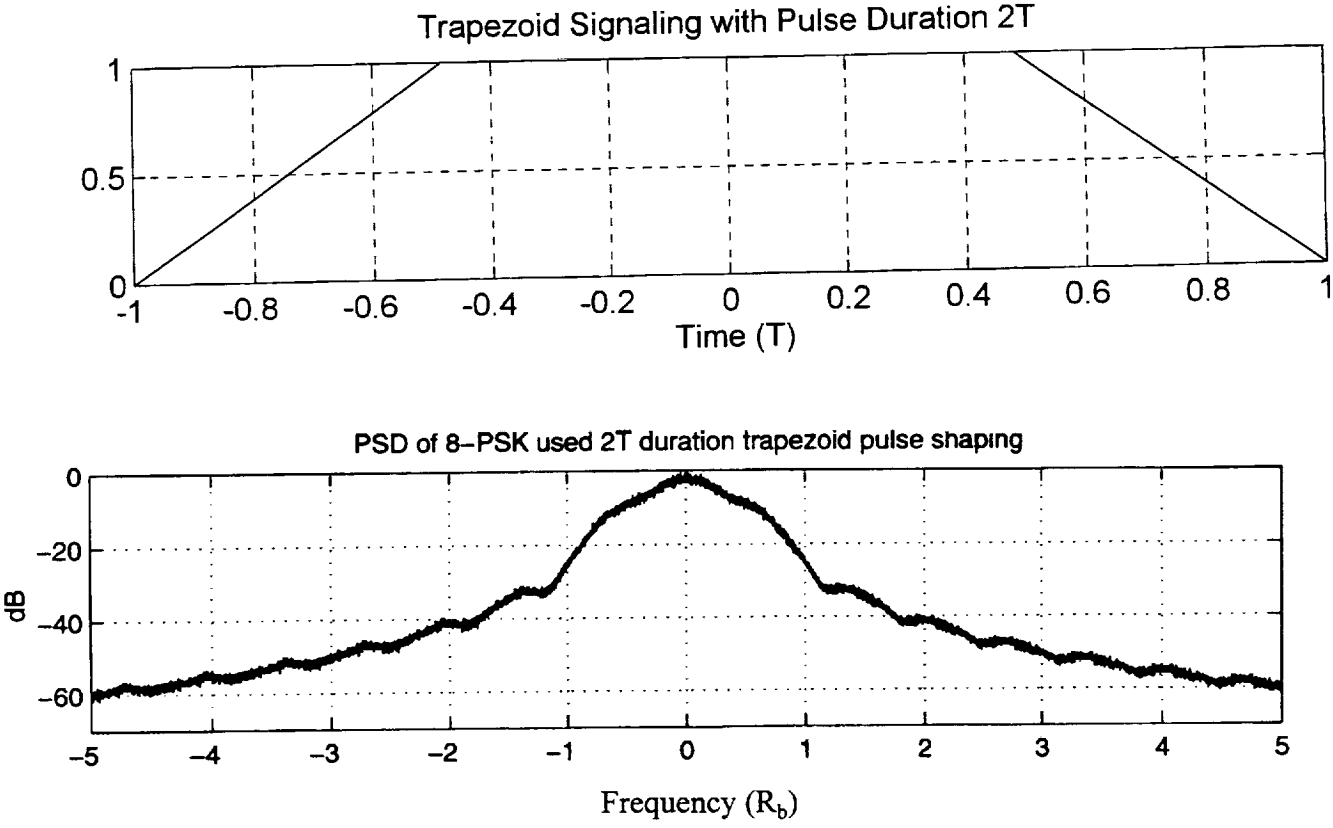

Figure 3-15 PSD of 8-PSK Used 2T Duration Trapezoid Pulse Shaping

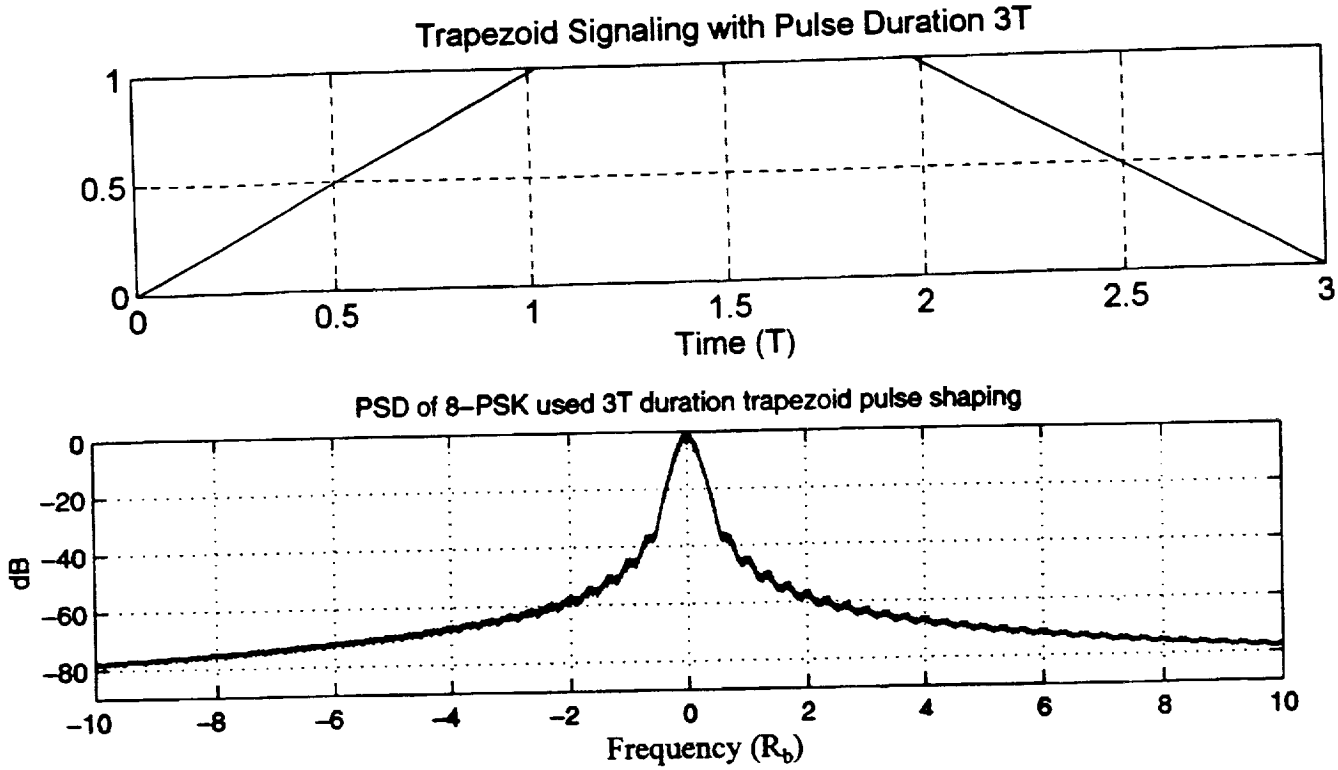

Figure 3-16 PSD of 8-PSK used 3T-s duration trapezoid pulse shaping

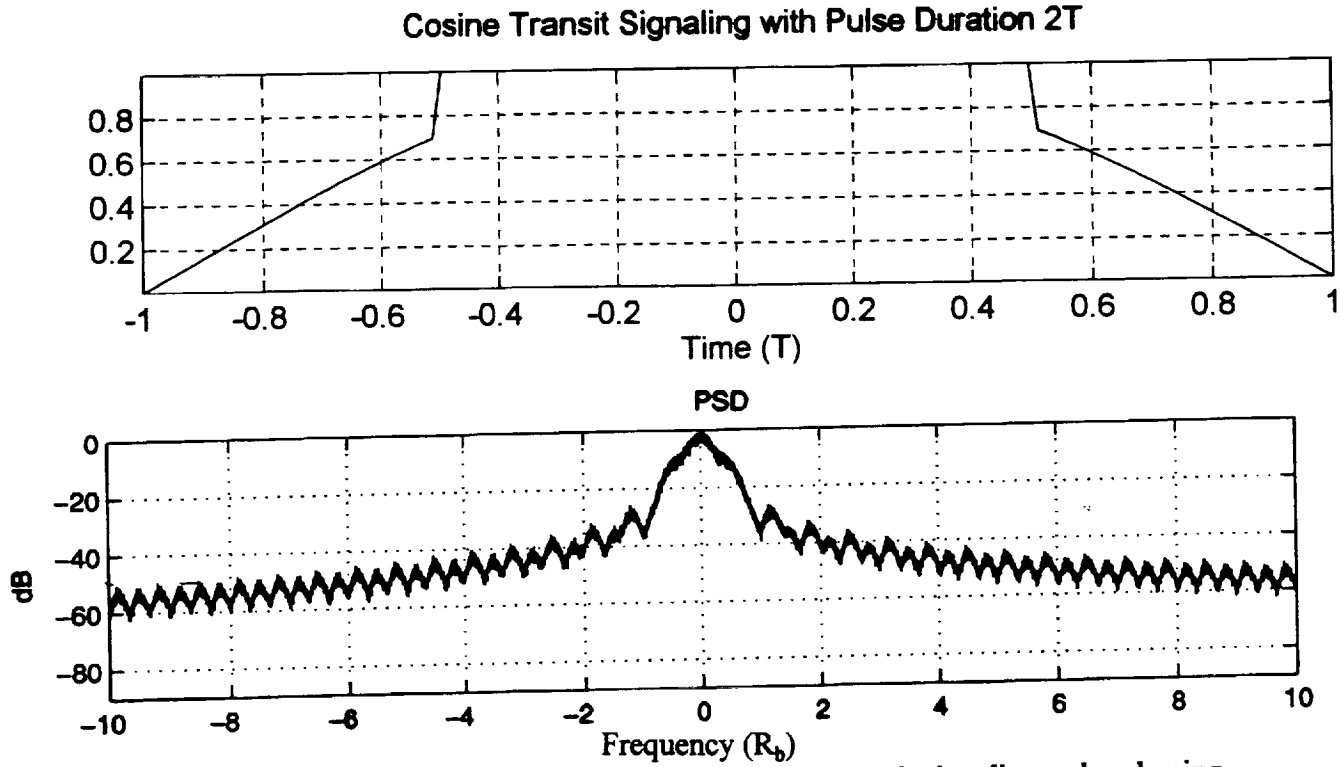

Figure 3-17 PSD of 8-PSK used 2T-s duration cosine transit signaling pulse shaping

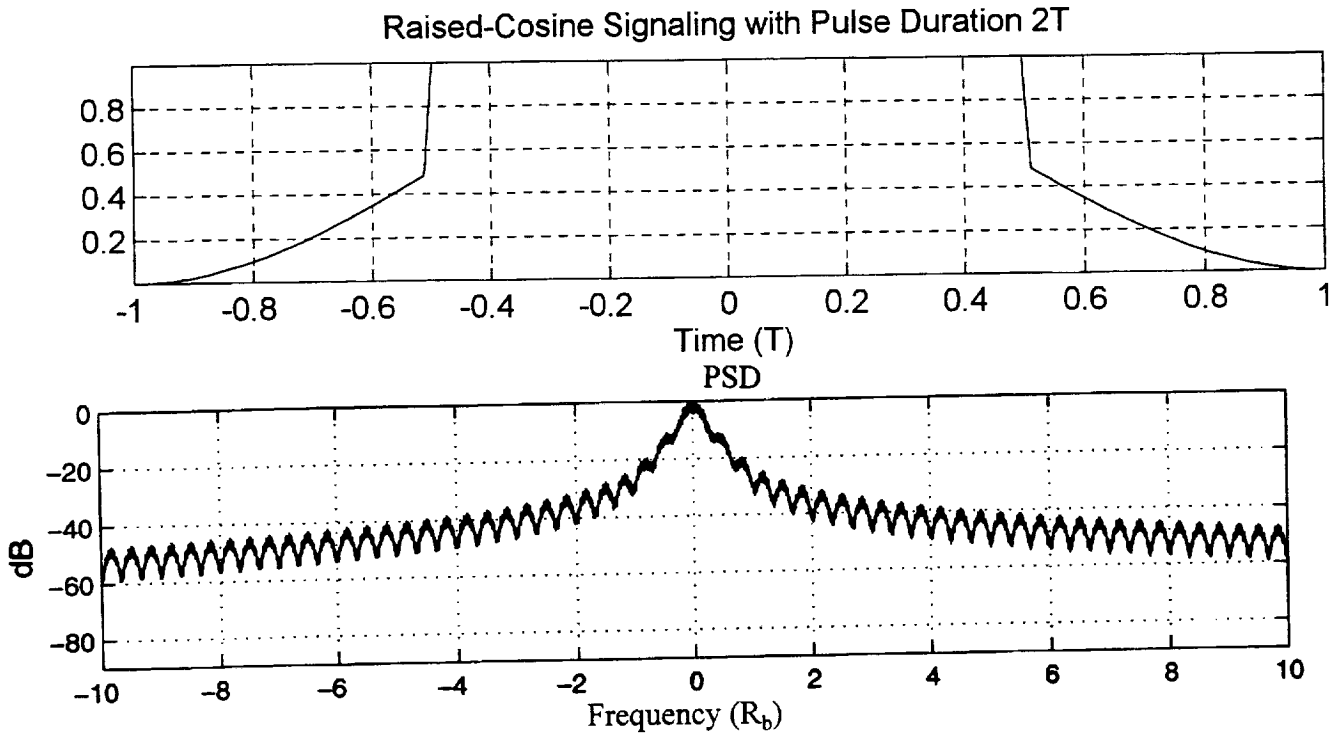

Figure 3-18 PSD of 8-PSK Used 2T Raised Cosine Transit Signaling Pulse Shaping

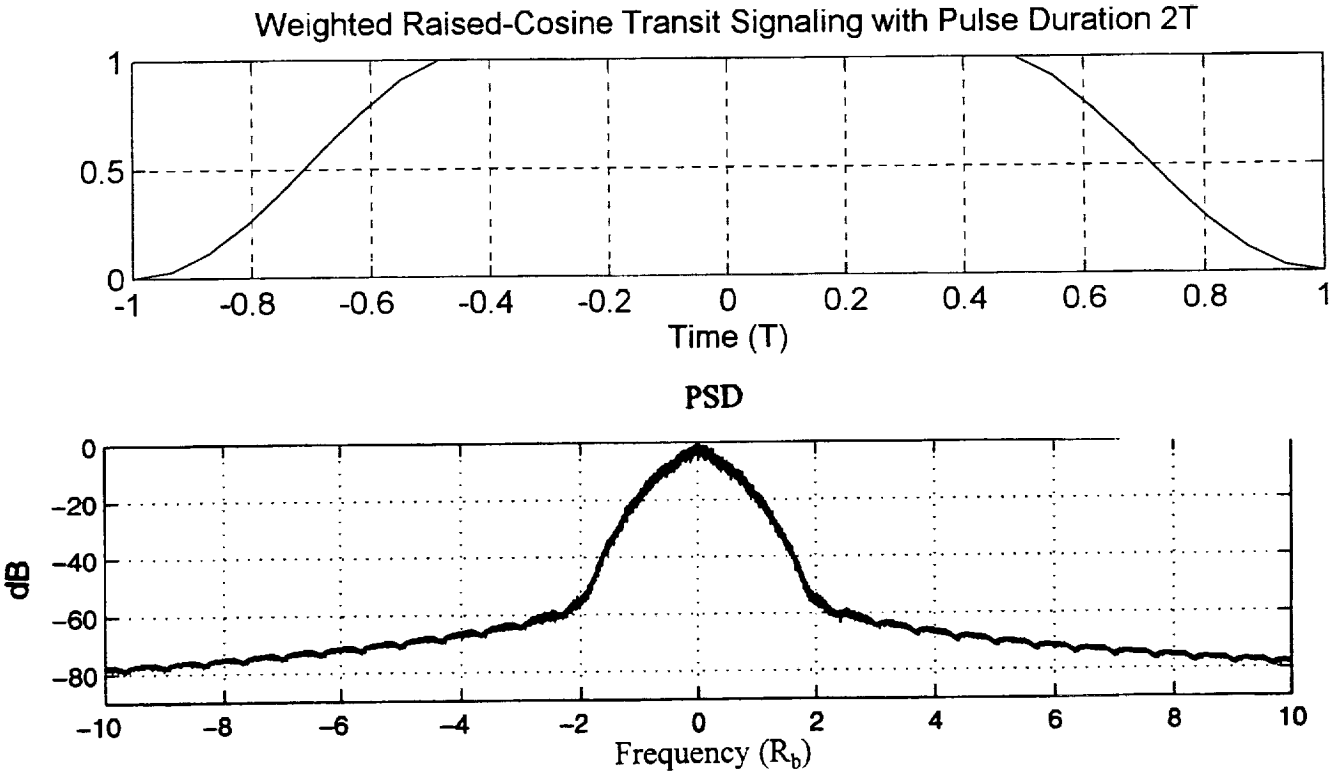

Figure 3-19 PSD of 8-PSK Used 2T Duration
Weighted Raised Cosine Transit Signaling Pulse Shaping

3.1.4 Analysis Results of Particular 8-PSK Waveforms

According to formula (2-38) and (2-39), numerical analysis results of PSD for trapezoid and weighted raised cosine signaling at some particular frequencies have been calculated and are shown in Table 3-4 and Table 3-5. The discrete line components are virtually zero, and they can eliminate all spikes. Simon's recent report [3] also indicated 3T duration trapezoid can eliminate power spectral line components. Tables 3-6 and Table 3-7 show that the raised cosine and cosine transit signaling can reduce line components, but could not get rid of them. Analysis results are consist with simulation results.

Table 3-4 PSD Line Components for Trapezoid Shaping

fT	0	1	2	3	4
PSD	0.0819×10^{-32}	0.0048×10^{-32}	0.0048×10^{-32}	0.0098×10^{-32}	0.0091×10^{-32}

Table 3-5 PSD Line Components for Weighted Raised Cosine Shaping

fT	0	1	2	3	4
PSD	0.1736×10^{-32}	0.0217×10^{-32}	0.0087×10^{-32}	0.0164×10^{-32}	0.0052×10^{-32}

Table 3-6 PSD Line Components for Raised Cosine Transit Shaping

fT	0	1	2	3	4
PSD	4.213×10^{-4}	4.213×10^{-4}	4.213×10^{-4}	4.213×10^{-4}	4.213×10^{-4}

Table 3-7 PSD Line Components for Cosine Transit Shaping

fT	0	1	2	3	4
PSD	4.333×10^{-5}	4.333×10^{-5}	4.333×10^{-5}	4.333×10^{-5}	4.333×10^{-5}

From the simulations, the utilization ratios of pre-modulation pulse shaping with these waveforms were calculated and listed in Table 3-8 and Figure 3-20

Table 3-8 Utilization Ratio of Pre-Modulation Pulse Shaping 8-PSK with Different Waveforms

Pulse Types	**-50 dB point (R_b)**	**Utilization**
None	35	1
2T-s Trapezoid Pulses	3	11.6
3T-s Trapezoid Pulses	1	35
2T-s Pulses with Cosine Transit	7.5	4.6
2T-s Pulses with Raise-Cosine Transit	10	3.5
2T-s Pulses with Weighted Raised-Cosine Transit (k=1.5)	1.8	19.4

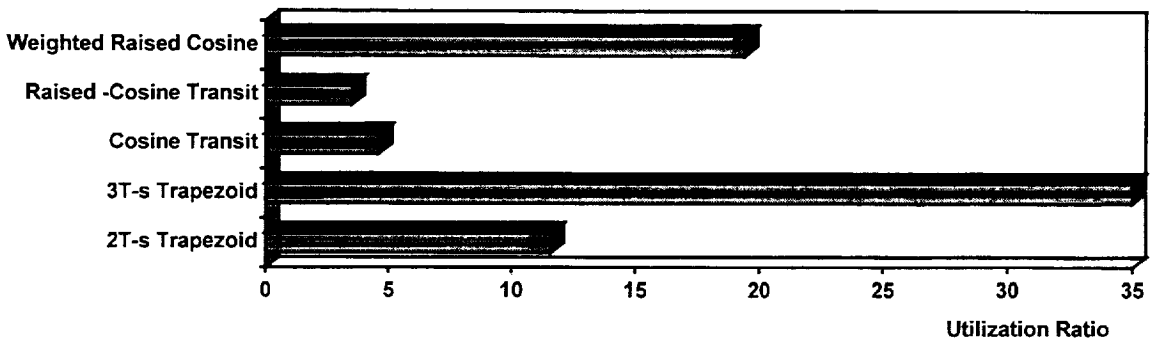

Figure 3-20 Utilization Ratio of Different Pulses in Pre-Modulation Pulse Shaping

3.2 Bit Errors Rates Simulations

Figure 3-21 shows the system block diagram for pulse shaped 8-PSK end to end system simulations.

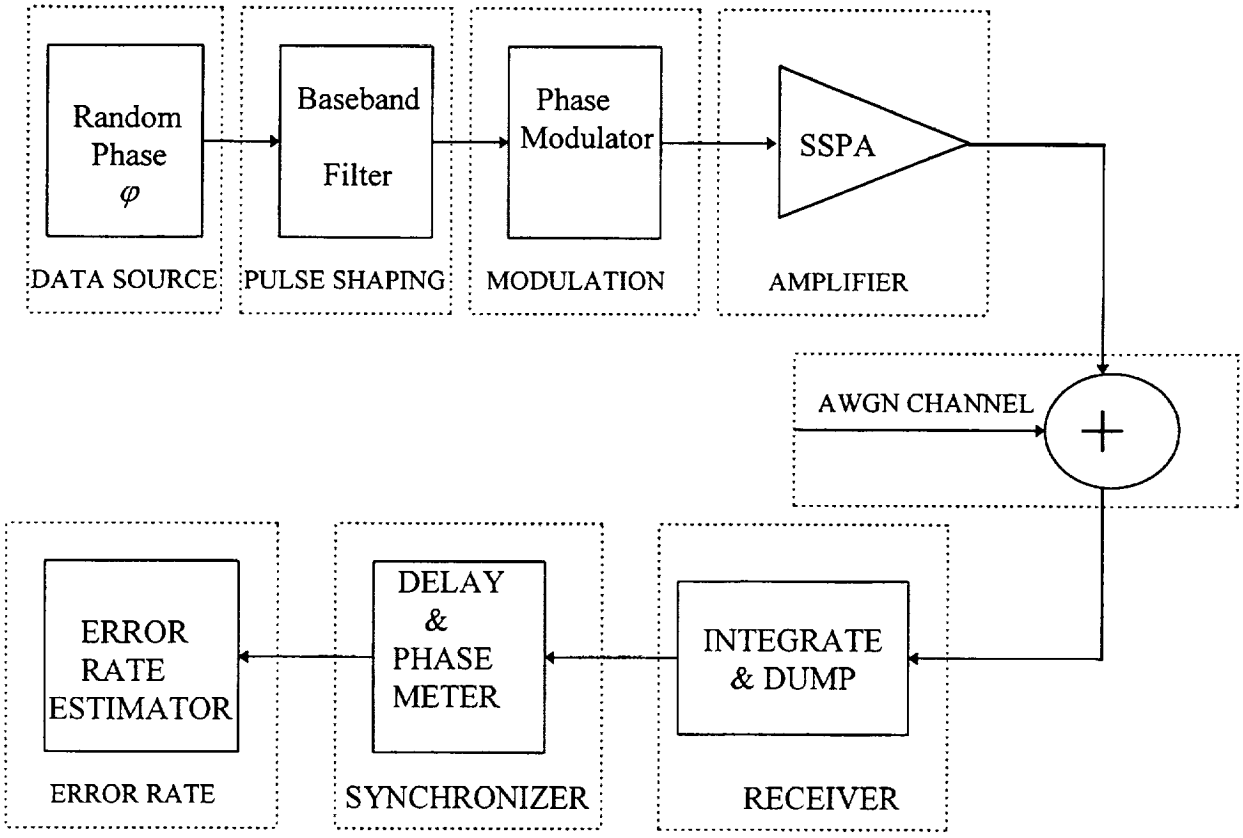

Figure 3-21 BER Simulation System Block Diagram

AWGN is added to the signals out of the SSPA to simulate channel noise. The bit errors are produced due to the ISI and AWGN. This report provides the measure of bit errors according to bit energy to noise ratio (Eb/N_o). Figure 3-21 shows the system block diagram for measuring bit error rates. For different pre-modulation pulse shaping filters with the same BT, the plots of the BER are in Figure 3-22 to Figure 3-24 .

The following parameters were used to obtain the bit error rates:

Data source:

a. Ideal data with p(0) (probability of zero)=0.5;

c. Symbol rate R_s=1

b. Sample Rate (f_s) = $16R_s$

Pulse Shaping Filters:

a. Butterworth 5th Order (BT=1,2,2.8,3)

b. Bessel 3rd Order (BT=1,1.2,2,3)

c. SRRC(α =1,Number of tap length=$256R_s$, rectangular window)

Power Amplifier:

European Space Agency(ESA) 10-watt SSPA, Back off =0dB as obtained from JPL

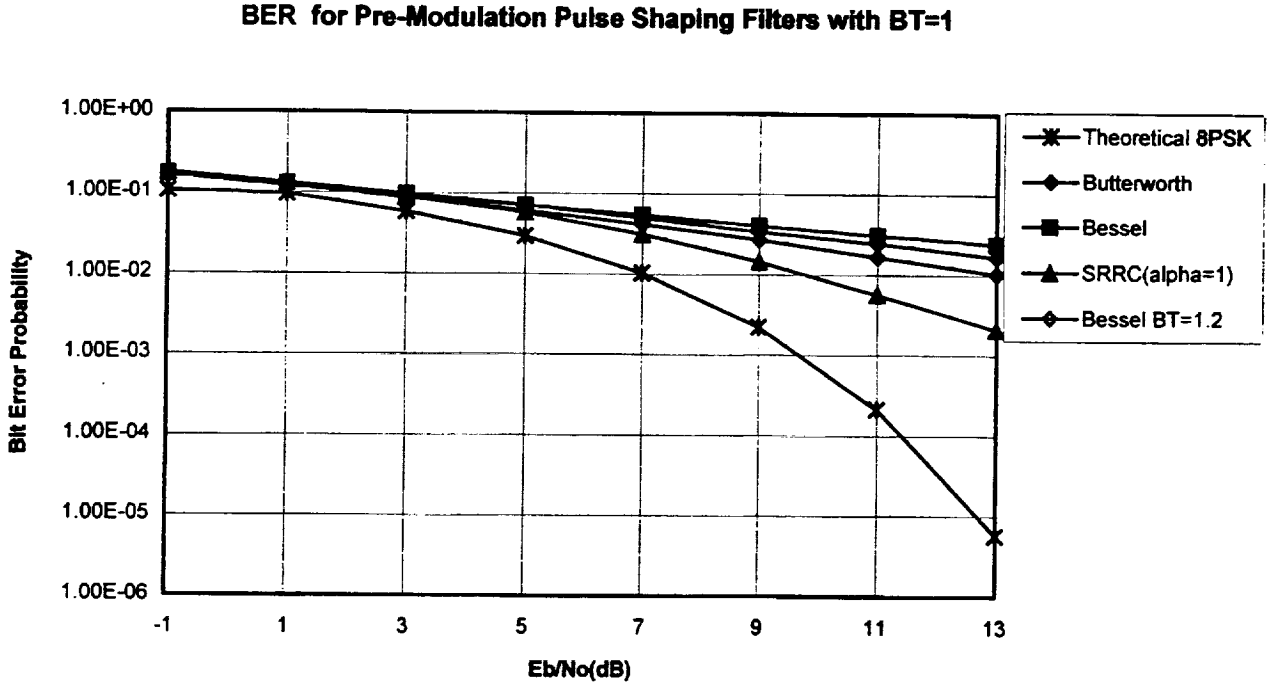

Figure 3-22. BER Plot for Pre-Modulation Pulse Shaping Filters with BT=1

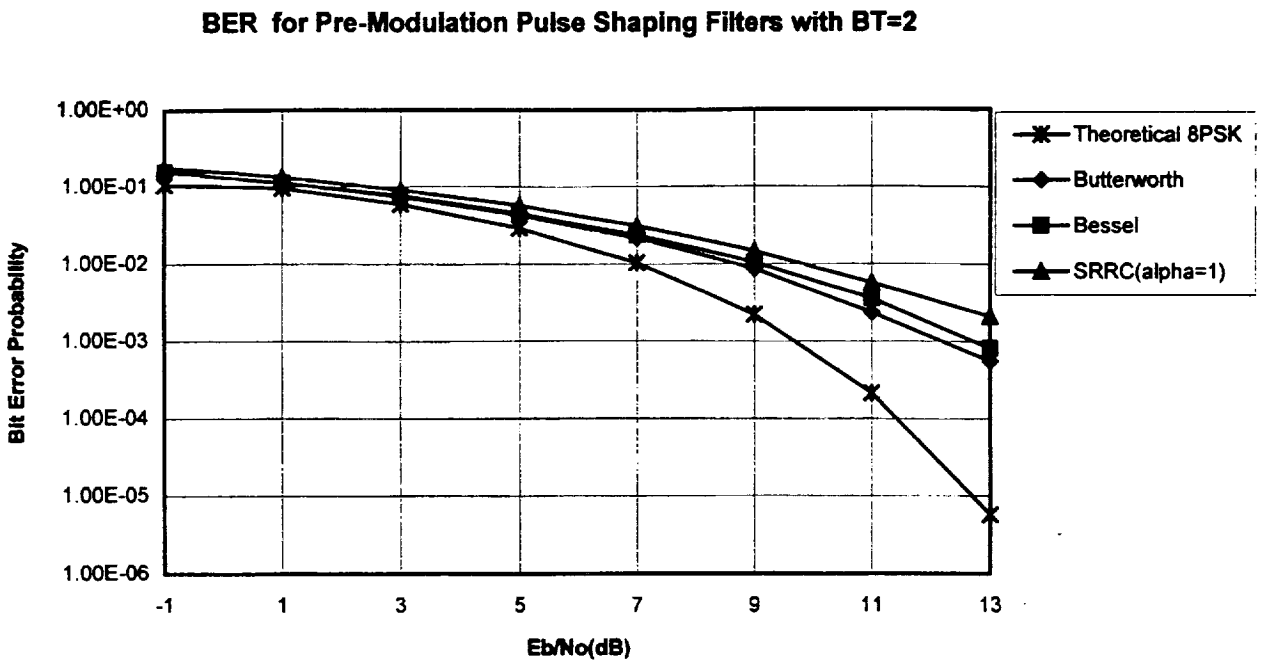

Figure 3-23. BER Plot for Pre-Modulation Pulse Shaping Filters with BT=2

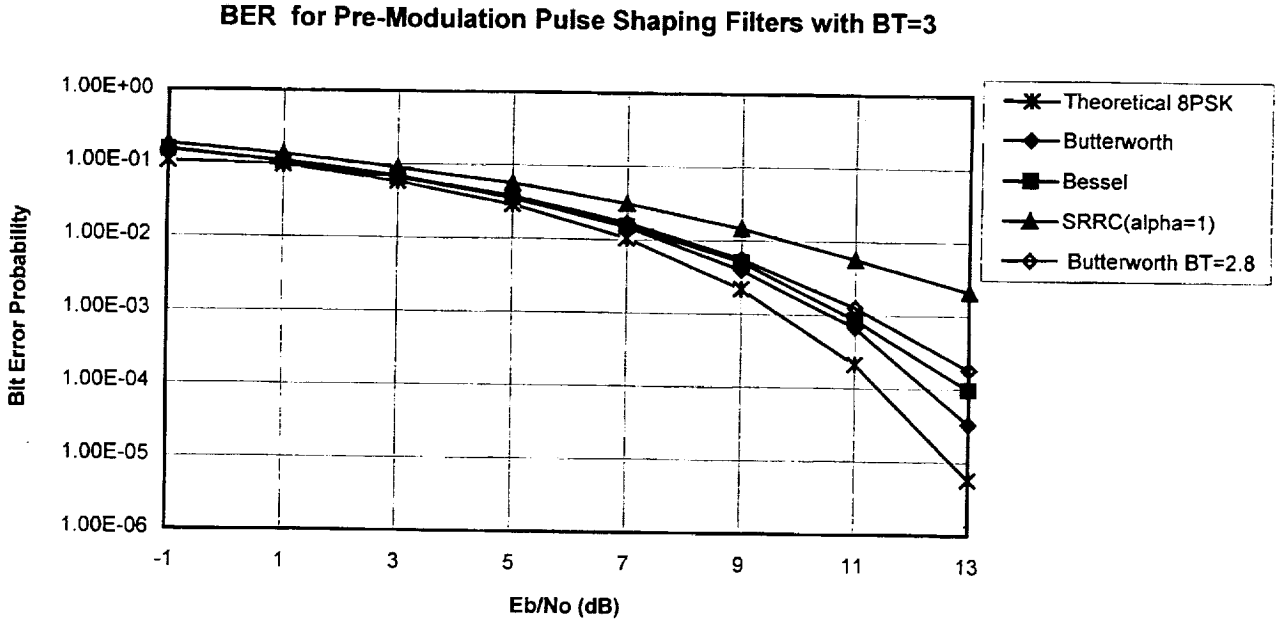

Figure 3-24. BER Plot for Pre-Modulation Pulse Shaping Filters with BT=3

Although the Utilization ratio (Figure 3-20) for 3T Trapezoid is very high and the power spectra are no spikes (Figure 3-6) , this kind of waveform has overlapping within 3 symbol periods. This overlapping introduce a very serious ISI such that the integrate and dump circuit can not work. Figure 3-25 shows the BER of pre-modulation pulse shaping by using 3T Trapezoid. Since this BER is not accepted, other kind of receiver should be used to correct ISI. An equalizer or sequential detector may be used to improve BER performance.

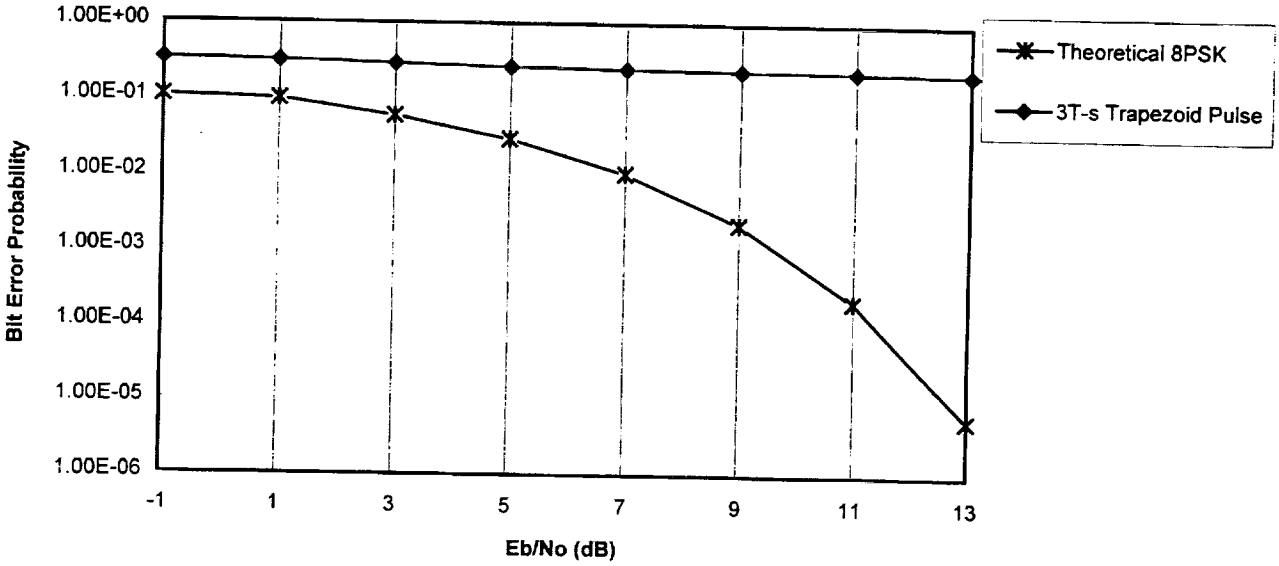

Figure 3-25. BER Plot for Pre-Modulation Pulse Shaping With 3T Trapezoid Signaling

ISI Losses Due to Filtering

The ISI losses due to the pulse shaping filters can be determined by the BER simulations. One needs to note that the receiver here was not an optimal receiver. Since the

integrate and dump was used as receiver, it could not matched the pulse shaped signals. Furthermore, there was no equalization for correcting ISI. The following tables give the results of baseband filter ISI losses at 10^{-3} BER for theoretical 8-PSK(or BPSK) [7] and the filtered 8-PSK.

Table 3-9 ISI Loss Measurements at 10^{-3} BER (Compared to ideal 8PSK)

Filter Type	Loss BT=1 (dB)	Loss BT=1.2 (dB)	Loss BT=2 (dB)	Loss BT=2.8 (dB)	Loss BT=3 (dB)
Butterworth 5th Order	12.5	----------	2.32	1.48	1.48
Bessel 3rd Order	----------	10	2.85	----------	1.20
SRRC(α=1)	4.22	----------	----------	----------	----------

Table 3-10 ISI Loss Measurements at 10^{-3} BER (Compared to ideal BPSK)

Filter Type	Loss BT=1 (dB)	Loss BT=1.2 (dB)	Loss BT=2 (dB)	Loss BT=2.8 (dB)	Loss BT=3 (dB)
Butterworth 5th Order	15.7	----------	5.52	4.68	4.68
Bessel 3rd Order	----------	13.2	6.05	----------	4.88
SRRC(α=1)	7.42	----------	----------	----------	----------

As stipulated in [16], the optimum filter should have the smallest BT value and provide losses<0.4 dB. Thus an ideal matched filter and equalizer should be applied to meet the

requirement of ISI loss <0.4. The Figure 3-25 shows the relationship of ISI loss and utilization ratio for different filters.

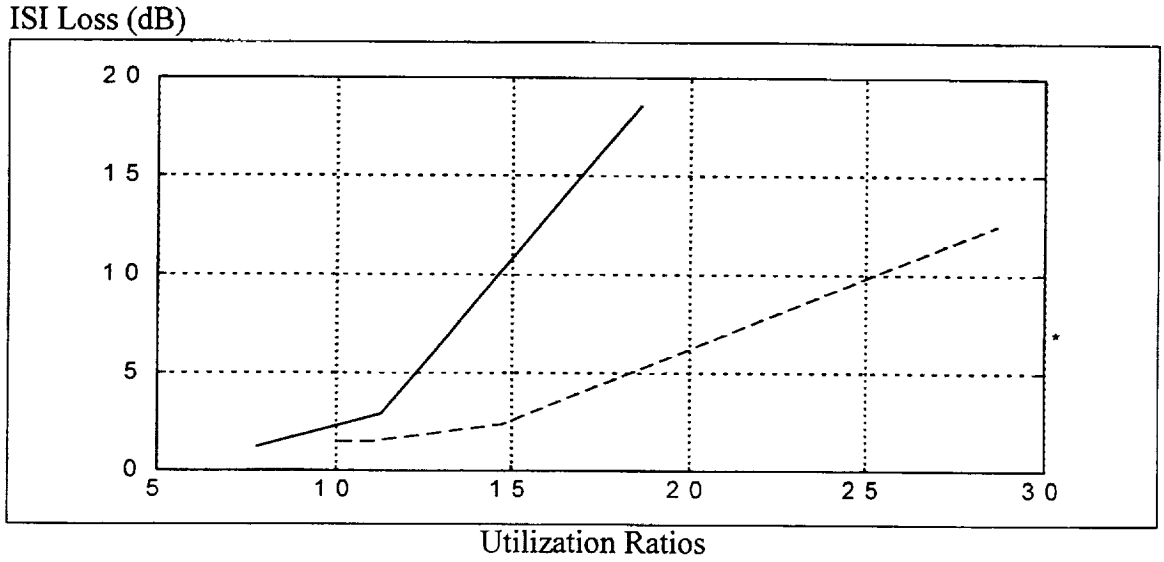

Figure 3-25. Plots for ISI Loss as Utilization Ratios for Pre-Modulation Pulse Shaping (------ for 5th Order Butterworth Filter ; ..... for 3rd Order Bessel Filter; * for SRRC filter)

Chapter 4

CONCLUSIONS AND RECOMMENDATIONS

This simulation based investigation on the pulse shaped 8-PSK modulations lead to the following conclusions.

Pulse shaping is an effective way to reduce bandwidth and cope with the increasing congestion of frequency band. Pre-modulation pulse shaping can keep constant envelope and is more efficient on narrowing bandwidth than post-modulation pulse shaping. On the other hand, pre-modulation pulse shaping using Butterworth, Bessel and SRRC filters can produce discrete spectral components, and using integrate and dump receiver could not ideally match pulse shaped signals. Thus the BER simulations by the pre-modulation pulse shaping method are a best-case scenario. In order to reduce power spectral spikes and improve BER, specialized 8-PSK pulse waveforms have been studied.

Pre-modulation pulse shaping and post-modulation pulse shaping have different effects on narrowing bandwidth or frequency band utilization ratio. In general, pre-modulation pulse shaping had better results for narrowing the bandwidth than post-modulation pulse shaping did for the same traditional filters and BT values due to the spectrum spreading effect of a non-constant modules through the non-linear amplifier.

Pre-modulation pulse shaping and post-modulation pulse shaping also have different effects on producing bit error rates. In general, post-modulation pulse shaping had lower bit error rates than pre-modulation pulse shaping for the non-ideal integrate & dump receiver. That means that the narrower the bandwidth, the larger the bit error rate. For the 3rd Order Bessel filter, the BER produced by post-modulation pulse shaping (BT=2) is

almost the same as that produced by pre-modulation pulse shaping (BT=3). For the 5th Order Butterworth filters, the BER produced by pre-modulation pulse shaping (BT=2.8 or 3) is between those produced by post-modulation pulse shaping BT=1 and BT =2.

Several pulse waveforms have been simulated, the pulse with cosine and raised cosine can reduce power spectral line components. Furthermore, simulation and analysis have shown that trapezoid and the pulse with weighted raised cosine transit can get rid of discrete spectrum. Simon[3] and simulations also indicated that keeping at least one symbol period flat and changing pulse transit can generate different effect on narrowing bandwidth with no discrete spectrum. For further study, an improved method may be found to change the pulse transit such that an optimal bandwidth with no spikes can be achieved. On the other hand, any such method may also introduce potentially severe ISI.

A matched filter is crucial for receiving the signal to lower the BER. Matched filters which can match pre- modulation pulse shaped signals are needed so that the BER can be reduced. Since trapezoid and the pulse with weighted raised cosine transit have been found to eliminate power spectral spikes, and they have deterministic waveforms which have at least two symbol period duration, matched filters can be obtained according to these waveforms.

Pulse shaping methods can introduce ISI and increasing BER. In order to obtain better performance on BER, in addition to using an ideal matched filter, an equalizer may be needed to reduce ISI.

REFERENCE

[1] V. K. Prabhu and H. E. Rowe, "Spectra of Digital Phase Modulation by Matrix Methods," *Bell Syst. Tech. J.*, vol. 53, pp. 899-935, May/June 1974.

[2] M. K. Simon, "On the Power Spectrum of Angle-Modulated PSK Signals Corrupted by ISI," *Private Communication,* pp. 1-7, March 1996.

[3] M. K. Simon, "On the Power Spectrum of Angle-Modulated PSK Signals Corrupted by Intersymbol Interference," *TDA Progress Report 42-131,* pp. 1-10, November 1997.

[4] L. J. Greenstein, "Spectra of PSK Signals with Overlapping Baseband Pulses," *IEEE Trans. Commun.*, vol. COM-25, pp. 523-530, May 1977.

[5] D. Subaainghe-Dias and K. Feher, "Baseband Pulse Shaping for $\pi/4$ FQPSK in Nonlinearly Amplified Mobile Channels," *IEEE Trans. Commun.*, vol. 42, pp. 2843-2852, October 1994.

[6] R. Caballero, "8-PSK Signaling over Non-Linear Satellite Channels," *Masters Thesis, New Mexico State University*, pp. 1-200, May 1996.

[7] P. J. Lee, "Computation of the Bit Error Rate of Coherent M-ary PSK with Gray code Bit Mapping," *IEEE Trans. Commun.*, vol. COM-34, pp. 488-491, May 1986.

[8] A. V. Oppenheim and R. W. Schafer, *Discrete-Time Signal Processing.* Englewood Cliffs, NJ: Prentice-Hall, 1989.

[9] J. G. Proakis, *Digital Communications.* New York: McGraw-Hill, 1995.

[10] *SPW - The DSP Framework Communications Library Reference.* Comdisco Systems Product Number: SPW8015, March 1994.

[11] *Signal Processing WorkSystem DSP Library Reference,* Alta Group of Cadence Design Systems, Inc. Product Number: SPW8015, March 1995.

[12] *Signal Processing WorkSystem Interactive Simulation Library Reference.* Alta Group of Cadence Design Systems, Inc. Product Number: SPW8015, March 1995.

[13] W. L. Martin and T. M. Nguyen, "*CCSDC - SFCG Efficient Modulation Methods Study, A Comparison of Modulation Schemes, Phase 1: Bandwidth Utilization (Response to SFCG Action Item 12/32),*" SFCG-13, Ottawa Canada, 13-21 October 1993.

[14] M. Otter, "*CCSDC - SFCG Efficient Modulation Methods Study, A Comparison of Modulation schemes, Phase 1b: A Comparison of QPSK, OQPSK, BPSK, and GMSK Modulation Systems (Response to SFCG Action Item 12/32),*" European Space Agency/ESOC, Member CCSDS Subpanel 1E, (RF and Modulation), June 1994.

[15] W. L. Martin and T. M. Nguyen, *"CCSDC - SFCG Efficient Modulation Methods Study, A Comparison of Modulation Schemes, Phase 2: Spectrum Shaping (Response to SFCG Action Item 12/32),"* SFCG Meeting, Rothenberg, Germany 14-23, September 1994.

[16] W. L. Martin, T. M. Nguyen, A. Anabtawi, S. M. Hinedi, L. V. Lam and M. M. Shihabi, *"CCSDC - SFCG Efficient Modulation Methods Study Phase 3: End-to-End System Performance,"* Jet Propulsion Laboratory, May 1995.

[17] S. Haykin, *Communication Systems.* New York: John Wiley & Sons, 1994.